

## Reply to Editor: H. Cloke

In the following please find the corrections and comments to the referee's response. For clarity, the comments of the referee were copied in black and our comments are in blue.

Sections taken from the updated manuscript are shown in *italic*. Now deleted parts are ~~crossed-out~~ and newly added parts are underlined.

### Comments to the Author:

The referee has stated that you have addressed their main concerns and is happy to proceed with publication.

This is a very interesting paper. I have just one remaining question which I think it would be important to address before publication, and I apologise that this was not picked up at first review. How did you arrive at your decision on which parameters to include in your analysis "To simulate a wide range of possible flow conditions and limit the degrees of freedom for the possible model realizations we selected  $K_{sat}$  and porosity for calibration, while the Van Genuchten-Mualem parameters remained constant." Previous work I have carried out (Cloke et al, 2008) has shown that these types of models can be sensitive to a range of parameters and I believe you have not carried out a full sensitivity analysis which does worry me slightly as this would impact upon your findings. How many parameters does the model actually have and how many have you varied? Could you comment on this briefly in a minor revision?

Reference:

### General replies:

We thank the editor to pointing us in this direction and we extended the respective section to account for the raised remarks.

*To simulate a wide range of possible flow conditions and limit the degrees of freedom for the possible model realizations we selected  $K_{sat}$  and porosity for calibration, while the Van Genuchten-Mualem parameters remained constant since measured pF curves where available. Even though not all sensitive parameters of the Richards equation controlling the flow regime where accounted for during the calibration process, we assume that the measured Van Genuchten-Mualem parameters alpha and n are in the good agreement with the actual flow characteristics of the soils. As typical for the application of the VanGenuchten - Mualem approach the tortuosity/connectivity coefficient remained constant throughout all model runs with a value of 0.5. Beside the 4 soil parameters shown in Tab. 1 and the upper and lower boundary conditions, only the 9 parameters of the Shuttleworth-Wallace equation Tab. 2 had to be set prior to each model run.*

### References used by the Editor:

Cloke, H. L., Pappenberger, F. and Renaud, J.-P. (2008), Multi-method global sensitivity analysis (MMGSA) for modelling floodplain hydrological processes. *Hydrol. Process.*, 22: 1660–1674. doi: 10.1002/hyp.6734

# Revised manuscript

1 **Stable water isotope tracing through hydrological models for**  
2 **disentangling runoff generation processes at the hillslope scale**

3

4 David Windhorst<sup>1</sup>, Philipp Kraft<sup>1</sup>, Edison Timbe<sup>1,2</sup>, Hans-Georg Frede<sup>1</sup>, Lutz Breuer<sup>1</sup>

5

6 [1] {Institute for Landscape Ecology and Resources Management (ILR), Research Centre for  
7 BioSystems, Land Use and Nutrition (IFZ), Justus-Liebig-Universität Gießen, Germany}

8 [2] {Grupo de Ciencias de la Tierra y del Ambiente, DIUC, Universidad de Cuenca,  
9 Ecuador}

10

11 Correspondence to: D. Windhorst ([david.windhorst@umwelt.uni-giessen.de](mailto:david.windhorst@umwelt.uni-giessen.de))

## 12 **Abstract**

13 Hillslopes are the dominant landscape components where incoming precipitation is  
14 transferred to become groundwater, streamflow or atmospheric water vapor. However,  
15 directly observing flux partitioning in the soil is almost impossible. Hydrological hillslope  
16 models are therefore being used to investigate the processes involved. Here we report on a  
17 modeling experiment using the Catchment Modeling Framework (CMF) where measured  
18 stable water isotopes in vertical soil profiles along a tropical mountainous grassland hillslope  
19 transect are traced through the model to resolve potential mixing processes. CMF simulates  
20 advective transport of stable water isotopes  $^{18}\text{O}$  and  $^2\text{H}$  based on the Richards equation within  
21 a fully distributed 2-D representation of the hillslope. The model successfully replicates the  
22 observed temporal pattern of soil water isotope profiles ( $R^2$  0.84 and NSE 0.42). Predicted  
23 flows are in good agreement with previous studies. We highlight the importance of  
24 groundwater recharge and shallow lateral subsurface flow, accounting for 50% and 16% of  
25 the total flow leaving the system, respectively. Surface runoff is negligible despite the steep  
26 slopes in the Ecuadorian study region.

27

## 28 **1 Introduction**

29 Delineating flow path in a hillslope is still a challenging task (Bronstert, 1999; McDonnell et  
30 al., 2007; Tetzlaff et al., 2008; Beven and Germann, 2013). Though a more complete  
31 understanding in the partitioning of incoming water to surface runoff, lateral subsurface flow  
32 components or percolation allows to better understand, for example, the impact of climate and  
33 land use change on hydrological processes. Models are often used to test different rainfall-  
34 runoff generation processes and the mixing of water in the soil (e.g. Kirkby, 1988; Weiler and  
35 McDonnell, 2004). Due to the prevailing measurement techniques and therefore the available

36 datasets it has become common practice to base the validation of modeled hillslope flow  
37 processes on quantitative data on storage change. In the simplest case, system wide storage  
38 changes are monitored by discharge and groundwater level measurements or, on more  
39 intensively instrumented hillslopes, the storage change of individual soil compartments is  
40 monitored by soil moisture sensors. In the typical 2-D flow regime of a slope, such models  
41 bear the necessity not only to account for the vertical but also for the lateral movements of  
42 water within the soil (Bronstert, 1999). Quantitative data on storage change in this regard are  
43 only suitable to account for the actual change in soil water volume, but not to assess the  
44 source or flow direction. Knowing tracer compositions of relevant hydrological components  
45 along a hillslope allows to account for mixing processes and thereby to delineate the actual  
46 source of the incoming water. Over the years a number of artificial, e.g. fluorescence tracers  
47 like Uranine, and natural tracers, e.g. chloride or stable water isotopes, have emerged. While  
48 the application of the artificial tracers is rather limited in space and time (Leibundgut et al.,  
49 2011), the latter ones can be used over a wide range of scales (Barthold et al., 2011; Genereux  
50 and Hooper, 1999; Leibundgut et al., 2011; Muñoz-Villers and McDonnell, 2012; Soulsby et  
51 al., 2003). Stable water isotopes such as oxygen-18 ( $^{18}\text{O}$ ) and hydrogen-2 ( $^2\text{H}$ ) are integral  
52 parts of water molecules and consequently ideal tracers of water. Over the last decades  
53 isotope tracer studies have proven to provide reliable results on varying scales (chamber, plot,  
54 hillslope to catchment scale) and surface types (open water, bare soils, vegetated areas) to  
55 delineate or describe flow processes under field experimental or laboratory conditions  
56 (Garvelmann et al., 2012; Hsieh et al., 1998; Sklash et al., 1976; Vogel et al., 2010;  
57 Zimmermann et al., 1968).

58 Although the first 1d process orientated models to describe the dynamics of stable water  
59 isotope profiles for open water bodies (Craig and Gordon, 1965) and a bit later for soils  
60 (Zimmermann et al., 1968) have been developed as early as in the mid 1960's, fully  
61 distributed 2-D to 3-D hydrological tracer models benefitting from the additional information

62 to be gained by stable water isotopes are still in their early development stages (Davies et al.,  
63 2013) or use strong simplifications of the flow processes (e.g. TAC<sup>D</sup> using a kinematic wave  
64 approach; Uhlenbrook et al., 2004). This can be attributed to the high number of interwoven  
65 processes affecting the soil water isotope fluxes not only in the soil's liquid phase but also in  
66 its vapor phase. The more process based 1d models (Braud et al., 2005; Haverd and Cuntz,  
67 2010) therefore simultaneously solve the heat balance and the mass balance simultaneously  
68 for the liquid and the vapor phase and are thereby describing the:

- 69 • convection and molecular diffusion in the liquid and vapor phase,
- 70 • equilibrium fractionation between liquid and vapor phase,
- 71 • fractionation due to evaporation, and
- 72 • non-fractionated flux due to percolation and transpiration.

73 To obtain and compute the data required to apply these kind of models beyond the plot scale  
74 is still challenging. However, due to emerging measuring techniques the availability of  
75 sufficient data becomes currently more realistic. Increasing computational power and  
76 especially the cavity ring-down spectroscopy (CRDS) - a precise and cost effective method to  
77 analyze the signature of stable water isotopes (Wheeler et al., 1998) - promise progress.

78 Hence, it is tempting to investigate the suitability of isotope tracers to delineate hydrological  
79 flow paths using a more physical modeling approach. Recent research in this direction  
80 includes the work of McMillan et al. (2012) and Hrachowitz et al. (2013) using chloride as a  
81 tracer to study the fate of water in catchments in the Scottish Highlands. Even though some  
82 processes affecting the soil water isotope transport are still represented in a simplified manner  
83 or could be , due to their limited effect/importance of the respective process within the given  
84 study site, omitted, this approach allows us to determine the potential of soil water isotope  
85 modeling in catchment hydrology and highlight future need for research.

86 This study is conducted in a 75 km<sup>2</sup> montane rain forest catchment in south Ecuador, the  
87 upper part of the Rio San Francisco, which has been under investigation since 2007 (Bogner  
88 et al., 2014; Boy et al., 2008; Bücken et al., 2011; Crespo et al., 2012; Fleischbein et al., 2006;  
89 Goller et al., 2005; Timbe et al., 2014; Windhorst et al., 2013b). The findings of those studies  
90 (briefly synthesized in section 2.3) will a) ease the setup of chosen model, b) let us define  
91 suitable boundary conditions for the chosen modeling approach and c) serve as a reference for  
92 the delineated flow bath. The additional information from previous studies conducted in the  
93 study area, will therefore highlight the potential of this new model approach to delineate  
94 hydrological flow paths under natural conditions and support our preliminary hydrological  
95 process understanding retrieved from more classical methods conducted in the past.

96 Within this catchment we selected a hillslope with a distinct drainage area and nearly  
97 homogenous land-use and established an experimental sampling scheme to monitor the  
98 isotopic signatures of the soil water of three soil profiles using passive capillary fiberglass  
99 wick samplers (PCaps). Based on the proposed modeling approach a 2-D virtual hillslope  
100 representation of this hillslope was then implemented using the Catchment Modeling  
101 Framework (CMF; Kraft et al., 2011). Due to the necessity to mix the flows in accordance to  
102 the observed soil water isotope signatures we are confident, that the degree of certainty for the  
103 modeled flow path will be higher, than for conventional modeling approaches relying solely  
104 on quantitative information to evaluate the modeled data. Replacing the calibration target  
105 bears now the necessity to mix the right amount and signature of any given flow component,  
106 whereas the quantitative change only relies on the actual amount of water leaving or entering  
107 any given compartment. We will quantify the following flow components to disentangle the  
108 runoff generation processes: surface runoff, lateral subsurface flow in the vadose zone and  
109 percolation to groundwater. The lateral subsurface flow will be further subdivided into near  
110 surface lateral flow and deep lateral flow.

111 To validate the chosen modeling approach and assess our process understanding we tested the  
112 following hypotheses:

- 113 I. Under the given environmental conditions - high precipitation and humidity -  
114 (Bendix et al., 2008) and full vegetation cover (Dohnal et al., 2012; Vogel et al.,  
115 2010) only non-fractionating and advective water transport of isotopes is relevant.  
116 Gaseous advection and diffusive process in the gaseous as well as the liquid phase  
117 and the enrichment due to evaporation are negligible; hence the stable water  
118 isotopes behave like a conservative tracer.
- 119 II. Large shares of the soil water percolate to deeper horizons, thereby creating long  
120 mean transit times (MTT) (Crespo et al., 2012; Timbe et al., 2014).
- 121 III. Due to the high saturated conductivities of the top soil layers the occurrence of  
122 Hortonian overland flow is unlikely to have an important contribution to the  
123 observed flows (Crespo et al., 2012)
- 124 IV. Fast near surface lateral flow contributes essentially to downhill water flows and  
125 play a relevant role to understand the overall hydrological system (Bücker et al.,  
126 2010).

127

## 128 **2 Materials and Methods**

### 129 **2.1 Study area**

130 The hillslope under investigation is located within the catchment of the Rio San Francisco in  
131 South Ecuador ( $3^{\circ}58'30''\text{S}$ ,  $79^{\circ}4'25''\text{W}$ ) at the eastern outskirts of the Andes and  
132 encompasses an area of  $75 \text{ km}^2$ . Close to the continental divide the landscape generally  
133 follows a continuous eastward decline towards the lowlands of the Amazon basin (Figure 1b).  
134 Due to the high altitudes (1720-3155m a.s.l.), the deeply incised valleys (slopes are on

135 average 25°-40° over the entire watershed), the low population density and the partly  
136 protected areas of the Podocarpus National Park, the human impact within the catchment is  
137 relatively low. The southern flanks of the Rio San Francisco are covered by an almost pristine  
138 tropical mountain cloud forest and lie mostly within the Podocarpus National Park. At lower  
139 elevations the northern flanks have mostly been cleared by natural or slash-and-burn fires  
140 during the last decades and are now partially used for extensive pasture (*Setaria sphacelata*  
141 Schumach.), reforestation sites (*Pinus patula*), are covered by shrubs or invasive weeds  
142 (especially tropical bracken fern; *Pteridium aquilinum* L.). The climate exhibits a strong  
143 altitudinal gradient creating relatively low temperatures and high rainfall amounts (15.3°C  
144 and 2000 mm a<sup>-1</sup> at 1960 m a.s.l. to 9.5°C and >6000 mm a<sup>-1</sup> at 3180 m a.s.l.) with the main  
145 rainy season in the austral winter (Bendix et al., 2008). A comprehensive description of the  
146 soils, climate, geology and land use has been presented by Beck et al. (2008), Bendix et al.  
147 (2008) and Huwe et al. (2008).

## 148 **2.2 Experimental hillslope**

149 To test our understanding of hydrological processes within the study area we choose a  
150 hillslope with a nearly homogenous land use (Figure 1). It is located on an extensive pasture  
151 site with low intensity grazing by cows and dominated by *Setaria sphacelata*. *Setaria*  
152 *sphacelata* is an introduced tropical C4 grass species that forms a dense tussock grassland  
153 with a thick surface root mat (Rhoades et al., 2000). This grass is accustomed to high annual  
154 rainfall intensities (>750 mm a<sup>-1</sup>), has a low drought resistance and tolerates water logging to  
155 a greater extent than other tropical grass types (Colman and Wilson, 1960; Hacker and Jones,  
156 1969). The hillslope has a drainage area of 0.025 km<sup>2</sup>, a hypothetical length of the subsurface  
157 flow of 451 m and an elevation gradient of 157 m with an average slope of 19.2°. The soil  
158 catena of the slope was recorded by Pürckhauer sampling and soil pits. To investigate the  
159 passage of water through the hillslope a series of three wick sampler has been installed along  
160 the line of subsurface flow.

161 Climate forcing data with an hourly resolution of precipitation, air temperature, irradiation,  
162 wind speed and relative humidity was collected by the nearby (400 m) climate station “ECSF”  
163 at similar elevation. Isotopic forcing data was collected manually for every rainfall event from  
164 Oct 2010 until Dec 2012 using a Ø25 cm funnel located in close proximity of the chosen  
165 hillslope at 1900 m a.s.l. (Timbe et al., 2014). To prevent any isotopic fractionation after the  
166 end of a single rainfall event (defined as a period of 30min without further rainfall) all  
167 samples were directly sealed with a lid and stored within a week in 2mL amber glass bottles  
168 for subsequent analysis of the isotopic signature as described in section 2.4.1 (all samples  
169 <2ml were discarded).

### 170 **2.3 Current process understanding at the catchment scale**

171 The catchment of the Rio San Francisco has been under investigation since 2007 (Bücker et  
172 al., 2011; Crespo et al., 2012; Timbe et al., 2014; Windhorst et al., 2013b) and was  
173 complemented by a number of studies on forested micro catchments ( $\approx 0.1 \text{ km}^2$ ) within this  
174 catchment (Bogner et al., 2014; Boy et al., 2008; Fleischbein et al., 2006; Goller et al., 2005).  
175 Studies on both scales identify the similar hydrological processes to be active within the study  
176 area.

177 Studies on the micro scale (Boy et al., 2008; Goller et al., 2005), supported by solute data and  
178 end member mixing analysis at the meso scale (Bücker et al., 2011; Crespo et al., 2012),  
179 showed that fast ‘organic horizon flow’ in forested catchments dominates during discharge  
180 events, if the mineral soils are water saturated prior to the rainfall. Due to an abrupt change in  
181 saturated hydraulic conductivity ( $K_{\text{sat}}$ ) between the organic ( $38.9 \text{ m d}^{-1}$ ) and the near-surface  
182 mineral layer ( $0.15 \text{ m d}^{-1}$ ) this ‘organic horizon flow’ can contribute up to 78% to the total  
183 discharge during storm events (Fleischbein et al., 2006; Goller et al., 2005). However, the  
184 overall importance of this ‘organic horizon flow’ is still disputable, because the rainfall  
185 intensity rarely gets close to such a high saturated hydraulic conductivity. In 95% of the

186 measured rainfall events between Jun 2010 and Oct 2012 the intensity was below  $0.1 \text{ m d}^{-1}$   
187 ( $\approx 4.1 \text{ mm h}^{-1}$ ) and was therefore 15 times lower than the saturated hydraulic conductivity of  
188 the mineral soil layer below the organic layer under forest vegetation and around 30 times  
189 lower than the saturated hydraulic conductivity of the top soil under pasture vegetation  
190 (Zimmermann and Elsenbeer, 2008; Crespo et al., 2012). The same conclusion holds true for  
191 the occurrence of surface runoff due to infiltration access on pasture (lacking a significant  
192 organic layer). Solely based on rainfall intensities surface runoff is therefore relatively  
193 unlikely to contribute to a larger extend in rainfall-runoff generation. The reported  $K_{\text{sat}}$  values  
194 are based on measurements of  $250 \text{ cm}^3$  undisturbed soil core samples vertically extracted  
195 from the center of each respective layer. Due to the chosen sampling method and the limited  
196 size of the soil cores the effective saturated hydraulic conductivity will be even higher and can  
197 vary for the horizontal flow component. When and to which extent a subsurface saturated  
198 prior the rainfall event would still trigger surface runoff on pastures therefore remains to be  
199 investigated.

200 Bückner et al. (2010) and Timbe et al. (2014) could show that base flow on the other hand has  
201 a rather large influence on the annual discharge volume across different land use types,  
202 accounting for  $>70\%$  and  $>85\%$ , respectively. These findings are also supported by the long  
203 mean transit time (MTT) of the base flow for different sub-catchments of the Rio San  
204 Francisco in comparison to the fast runoff reaction times, varying according to Timbe et al.  
205 (2014) between 2.1 and 3.9 years. Accordingly, the current findings confirm that the base  
206 flow – originating from deeper mineral soil and bedrock layers– is dominating the overall  
207 hydrological system in the study area (Crespo et al., 2012; Goller et al., 2005). Apart from this  
208 dominating source of base flow, Bückner et al. (2010) identified near surface lateral flow as a  
209 second component to be relevant for the generation of base flow for pasture sites.

## 210 2.4 Measurements

### 211 2.4.1 Passive capillary fiberglass wick samplers (PCaps)

212 We installed *passive capillary fiberglass wick samplers* (PCaps; short *wick samplers*,  
213 designed according to Mertens et al. (2007)) as soil water collectors at three locations along  
214 an altitudinal transects under pasture vegetation in three soil depths. PCaps maintain a fixed  
215 tension based on the type and length of wick (Mertens et al., 2007), require low maintenance  
216 and are most suitable to sample mobile soil water without altering its isotopic signature  
217 (Frisbee et al., 2010; Landon et al., 1999). We used woven and braided 3/8-inch fiberglass  
218 wicks (Amatex Co. Norristown, PA, US). 0.75 m of the 1.5 m wick was unraveled and placed  
219 over a 0.30 x 0.30 x 0.01 m square plastic plate, covered with fine grained parent soil material  
220 and then set in contact with the undisturbed soil.

221 Every collector was designed to sample water from three different soil depths (0.10, 0.25 and  
222 0.40 m) with the same suction, all having the same sampling area of 0.09 m<sup>2</sup>, wick type,  
223 hydraulic head of 0.3 m (vertical distance) and total wick length of 0.75 m. To simplify the  
224 collection of soil water the wick samplers drained into bottles placed inside a centralized tube  
225 with an inner diameter of 0.4 m and a depth of 1.0 m. To avoid any unnecessary alterations of  
226 the natural flow above the extraction area of the wick sampler the centralized tube was placed  
227 downhill and the plates were evenly spread uphill around the tube. A flexible silicon tube  
228 with a wall thickness of 5 mm was used to house the wick and to connect it to the 2 L  
229 sampling bottles storing the collected soil water. The silicon tube prevents evaporation and  
230 contamination of water flowing through the wick. Weekly bulk samples were collected over  
231 the period from Oct 2010 until Dec 2012 if the sample volume exceeded 2 mL. Soil water and  
232 the previously mentioned precipitation samples are analyzed using a cavity ring down  
233 spectrometer (CRDS) with a precision of 0.1 per mil for <sup>18</sup>O and 0.5 for <sup>2</sup>H (Picarro L1102-i,  
234 CA, US).

## 235 2.4.2 Soil survey

236 The basic soil and soil hydraulic properties for each distinct soil layer along the hillslope  
237 where investigated up to a depth of 2 m. Pürckhauer sampling for soil texture and succession  
238 of soil horizons was done every 25 m, while every 100 m soil pits were dug for sampling soil  
239 texture, soil water retention curves (pF-curves), porosity and succession of soil horizons. The  
240 results were grouped into 8 classes (Tab. 1) and assigned to the modeling mesh as shown in  
241 Figure 2. Retention curves (pF-curves) were represented by the *Van Genuchten-Mualem*  
242 function using the parameters  $\alpha$  and  $n$ .

243 All soils developed from the same parent material (clay schist) and are classified as Haplic  
244 Cambisol with varying soil thickness. Soil thickness generally increased downhill varying  
245 between 0.8 m and 1.8 m in depressions. Clay illuviation was more pronounced in the upper  
246 part of the hillslope (higher gradient in clay content) indicating lower conductivities in deeper  
247 soil layers.

## 248 2.5 Modeling

### 249 2.5.1 The Catchment Modeling Framework (CMF)

250 The Catchment Modeling Framework (CMF) developed by Kraft et al. (2011) is a modular  
251 hydrological model based on the concept of finite volume method introduced by Qu and  
252 Duffy (2007). Within CMF those finite volumes (e.g. soil water storages, streams) are linked  
253 by a series of flow accounting equations (e.g. Richards or Darcy equation) to a one to three  
254 dimensional representation of the real world hydrological system. The flexible set up of CMF  
255 and the variety of available flow accounting equations allows customizing the setup as  
256 required in the presented study. In addition to the water fluxes, the advective movement of  
257 tracers within a given system can be accounted for by CMF, making this modeling framework  
258 especially suitable to be used in our tracer study (Kraft et al., 2010). Starting with Beven and  
259 Germann (1982) scientist over the last decades frequently argued that Richards equation like

260 flow accounting equation assuming a time invariant and well mixed homogenous flow of  
261 water through the soil pore space, similar to those currently implemented in CMF, are not  
262 suitable to account for preferential flow relevant for modeling tracer transport (Brooks et al.,  
263 2010; Germann et al., 2007; Hrachowitz et al., 2013; Stumpp and Maloszewski, 2010). Being  
264 developed for the quantitative representation of soil water flow this equations cannot  
265 distinguish between water stored in different soil compartments (namely the soil matrix and  
266 macro pores) and only artificially try to represent macropore flow e.g. by favoring high  
267 saturated conductivity values or misshaped conductivity curves controlling the flow of water  
268 between soil compartments. Even though the capabilities of CMF to account for preferential  
269 flow are still in the development phase (e.g. by following the dual permeability approach in  
270 the future) and are not accounted for in the presented setup, our setup will once more  
271 highlight potential draw backs of the modeling approaches relying on Richards equation while  
272 modeling tracer transport at the hillslope scale.

### 273 **2.5.2 Setup of CMF**

274 To govern the water fluxes within our system we used the following flow accounting  
275 equations: Manning equation for surface water flow; Richards equation for a full 2-D  
276 representation of the subsurface flow; Shuttleworth-Wallace modification (Shuttleworth and  
277 Wallace, 1985) of the Penman-Monteith method to control evaporation and transpiration;  
278 constant Dirichlet boundary conditions representing the groundwater table and the outlet of  
279 the system as a rectangular ditch with a depth of 1.5 m. The lower boundary condition is only  
280 applicable if groundwater table is  $>2$  m below ground. Preliminary testing revealed that a  
281 discretization based on a constant vertical shift (5m) and alternating cell width increasing  
282 width depth (ranging from 1.25 cm to 83.75 cm) yielded the optimum model performance  
283 with regard to computing time and model quality. Based on 5 m contour lines (derived by  
284 local LIDAR measurements with a raster resolution of 1 m; using the Spatial Analyst package  
285 of ArcGis 10.1 from ESRI) this hillslope was further separated into 32 cells ranging in size

286 from 16.6 m<sup>2</sup> to 2,921.6 m<sup>2</sup> (Figure 1a). To account for small scale dynamics in the mixing  
287 process of stable water isotopes and to be able to run the model with a satisfactory speed, two  
288 different horizontal resolutions were used to discretize the each layer with depth. Layers  
289 encompassing wick samplers and their upslope neighbor were run with a finer resolution of at  
290 least 26 virtual soil layers increasing in thickness width depth (1x1.25 cm, 13 x 2.5 cm,  
291 7 x 5 cm and 5 x 10-50 cm). All other cells were calculated with coarser resolution of at least  
292 14 virtual soil layers (1 x 1.25 cm, 1 x 2.5 cm, 6 x 5 cm, 3 x 10 cm and 3 x 15-83.75 cm). In  
293 case the delineated soil type changed within a soil layer it was further subdivided according to  
294 Figure 2.

### 295 **2.5.3 Evapotranspiration**

296 Soil evaporation, evaporation of intercepted water and plant transpiration are calculated  
297 separately using the sparse canopy evapotranspiration method by Shuttleworth and Wallace  
298 (1985), in its modification by Federer et al. (2003) and Kraft et al. (2011). This approach  
299 requires the following parameterizations: soil surface wetness dependent resistance to extract  
300 water from the soil ( $r_{ss}$ ), the plant type dependent bulk stomatal resistance to extract water  
301 from the leaves ( $r_{sc}$ ), the aerodynamic resistances parameters ( $r_{aa}$ ,  $r_{as}$ , and  $r_{ac}$ ) for sparse crops  
302 as described by Shuttleworth and Gurney (1990) and Federer et al. (2003). Whereby  $r_{ac}$   
303 (Resistance Canopy Atmosphere) restricts the vapor movement between the leaves and the  
304 zero plane displacement height and  $r_{as}$  (Resistance Soil Atmosphere) restricts the vapor  
305 movement between the soil surface and the zero plane displacement height, which is the  
306 height of the mean canopy flow (Shuttleworth and Wallace, 1985; Thom, 1972). The  
307 aerodynamic resistances parameter  $r_{aa}$  refers to the resistance to move vapor between the zero  
308 plane displacement height and the reference height at which the available measurements were  
309 made. The necessary assumptions to parameterize the plant (*Setaria sphacelata*) and soil  
310 dependent parameters of the Shuttleworth-Wallace equation using the assumptions made by  
311 Federer et al. (2003) and Kraft et al. (2011) are listed in Tab. 2.

312 Furthermore, soil water extraction by evaporation is only affecting the top soil layer and soil  
313 water extraction by transpiration is directly controlled by root distribution at a certain soil  
314 depth. In accordance with field observations, we assumed an exponential decay of root mass  
315 with depth, whereby 90 % of the total root mass is concentrated in the top 0.20 m.

316

#### 317 **2.5.4 Calibration & Validation**

318 For calibration and validation purposes, we compared measured and modeled stable water  
319 isotope signatures of  $^2\text{H}$  and  $^{18}\text{O}$  of the soil water at each depths of the each wick sampler  
320 along the modeled hillslope. Hourly values of the modeled isotopic soil water signature were  
321 aggregated to represent the mean isotopic composition in between measurements ( $\approx 7$  days)  
322 and are reported in per mil relative to the Vienna Standard Mean Ocean Water (VSMOW)  
323 (Craig, 1961).

324 Literature and measured values for soil and plant parameters (Tab. 1 and Tab. 2) were used to  
325 derive the initial values for the calibration process. The initial states for calibration were  
326 retrieved by artificially running the model with those initial values for the first 2 years of the  
327 available dataset (Tab. 3). The results of this pre-calibration run were used as a starting point  
328 for all following calibration runs. A warm up period of 4 month (1.7.2010-31.10.10) preceded  
329 the calibration period (1.11.2010-31.10.2011) to adjust the model to the new parameter set.  
330 To simulate a wide range of possible flow conditions and limit the degrees of freedom for the  
331 possible model realizations we selected  $K_{\text{sat}}$  and porosity for calibration, while the *Van*  
332 *Genuchten-Mualem* parameters remained constant since measured pF curves where available.  
333 Even though not all sensitive parameters of the Richards equation controlling the flow regime  
334 where accounted for during the calibration process, we assume that the measured *Van*  
335 *Genuchten-Mualem* parameters alpha and n are in the good agreement with the actual flow  
336 characteristics of the soils. As typical for the application of the VanGenuchten - Mualem

337 approach the tortuosity/connectivity coefficient remained constant throughout all model runs  
338 with a value of 0.5. Beside the 4 soil parameters shown in Tab. 1 and the upper and lower the  
339 boundary conditions, only the 9 parameters of the Shuttleworth-Wallace equation Tab. 2 had  
340 to be set prior to each model run. To further control the unknown lower boundary condition  
341 and complement the calibration process, the suction induced by groundwater depth was  
342 changed for each calibration run.

343 To increase the efficiency of the calibration runs and evenly explore the given parameter  
344 space we used the Latin-Hyper cube method presented by McKay et al. (1979). The parameter  
345 range of each variable was therefore subdivided into 10 strata and sampled once using  
346 uniform distribution. All strata are then randomly matched to get the final parameter sets. A  
347 total of  $10^5$  parameter sets were generated for calibration with varying values for  $K_{sat}$  and  
348 porosity for all 8 soil types as well as different groundwater depths. An initial trial using  $10^4$   
349 parameter sets was used to narrow down the parameter range as specified in Tab. 4 for  $K_{sat}$   
350 and porosity for all 8 soil types and to 0 m to 100 m for the applicable groundwater depths.  
351 The performance of each parameter set was evaluated based on the goodness-of-fit criteria  
352 Nash-Sutcliffe efficiency (NSE) and the coefficient of determination ( $R^2$ ). In addition, the  
353 bias was calculated as an indicator for any systematic or structural deviation of the model.

354 After the calibration the best performing (“behavioral”) models according to a  $NSE > 0.15$ , an  
355 overall bias  $< \pm 20.0 \text{ ‰ } \delta^2\text{H}$  and a coefficient of determination  $R^2 > 0.65$ , were used for the  
356 validation period (Tab. 3) using the final states of the calibration period as initial values.

### 357 **3 Results and discussion**

#### 358 **3.1 Model performance**

359 In order to quantify the flow processes we first validated the overall suitability of the chosen  
360 model approach and the performance of the parameter sets. The parameter sets best

361 representing the isotope dynamics of  $\delta^2\text{H}$  (as previously defined as best performing  
362 (“behavioral”) parameter sets; same accounts for  $\delta^{18}\text{O}$ ; results are not shown) during the  
363 calibration period, explained the observed variation to even a higher degree during the  
364 validation period (average NSE 0.19 for calibration versus 0.35 for validation).

365 The linear correlation between modeled and observed isotope dynamics of  $\delta^2\text{H}$ , for the best  
366 performing parameter sets, were equally good during the calibration and validation period  
367 ( $R^2 \approx 0.66$ ) (Tab. 5). The goodness-of-fit criteria for the single best performing parameter set  
368 (“best model fit”) shows an  $R^2$  of 0.84 and a NSE of 0.42.

369 Figure 3 depicts the measured and modeled temporal development of the soil water isotope  
370 profile along the studied hillslope as well as the  $\delta^2\text{H}$  signature and amount of the incoming  
371 rainfall used to drive the model. The measured temporal delay of the incoming signal with  
372 depth and the general seasonal pattern of the  $\delta^2\text{H}$  signal are captured by the model (Figure 3).

373 The bias was negative throughout all model realizations during calibration and validation (-  
374 15.90 ( $\pm 0.11$  SD) ‰  $\delta^2\text{H}$  and -16.93 ( $\pm 0.34$  SD) ‰  $\delta^2\text{H}$  respectively see Tab. 5). Even though  
375 the high bias indicates a structural insufficiency of the model, we are confident that this can  
376 be mostly attributed by the discrimination of evaporation processes at the soil-atmosphere  
377 interface and on the canopy.

378 Our first hypothesis, that evaporation in general plays only a minor role for the soil water  
379 isotope cycle under full vegetation, therefore needs to be reconsidered. Even though  
380 hypothesis I has previously been frequently used as an untested assumption for various  
381 models (e.g. Vogel et al., 2010; Dohnal et al., 2012) it is rarely scrutinized under natural  
382 conditions. A complete rejection of this hypothesis could therefore affect the interpretations in  
383 those studies and limit their applicability. However, further studies are needed to support  
384 these findings and before finally rejecting this hypothesis. The lateral mixing processes maybe

385 obscuring the observed near surface enrichment and the effect of preferential flow currently  
386 not fully accounted for could further hinder the full interpretation of these findings. It still  
387 holds true, that:

- 388 - the quantitative loss due to surface evaporation on areas with a high leaf area index is  
389 more or less insignificant (accounting for  $38 \text{ mm a}^{-1}$  out of  $1,896 \text{ mm a}^{-1}$ ;  $\approx 2\%$ ; Figure 5),
- 390 - the isotopic enrichment due to evaporation for vegetated areas is considerably lower than  
391 for non-vegetated areas, as previously shown by Dubbert et al. (2013), and
- 392 - high rainfall intensity constrains any near surface isotopic enrichment related to  
393 evaporation (Hsieh et al., 1998).

394 However, our results indicate that the contribution of potential canopy evaporation  
395 (accounting for  $344 \text{ mm a}^{-1}$  out of  $1,896 \text{ mm a}^{-1}$ ;  $\approx 18\%$ ; Figure 5) to enrich the canopy storage  
396 and thereby potential throughfall (discriminating  $^{18}\text{O}$  and  $^2\text{H}$  resulting in more positive isotope  
397 signatures) still could partially explain the observed bias.

398 Nevertheless we presume that fog drip, created by sieving bypassing clouds or radiation fog  
399 frequently occurring in the study area Bendix et al. (2008), explains the majority of the  
400 observed bias. Depending on the climatic processes generating the fog drip is typically  
401 isotopically enriched compared to rainfall, due to different condensation temperatures (Scholl  
402 et al., 2009). To get an impression for the magnitude of the possible bias due to throughfall  
403 and fog drip compared to direct rainfall, we compare the observed bias with a study presented  
404 by Liu et al. (2007) conducted in a tropical seasonal rain forest in China. They observed an  
405 average enrichment of  $+5.5 \text{ ‰ } \delta^2\text{H}$  for throughfall and  $+45.3 \text{ ‰ } \delta^2\text{H}$  for fog drip compared  
406 to rainfall. Even though the observed enrichment of fog drip and throughfall by Liu et al.  
407 (2007) may not be as pronounced within our study area (Goller et al., 2005), the general  
408 tendency could explain the modeled bias. According to Bendix et al. (2008) fog and cloud  
409 water deposition within our study area contributes  $121 \text{ mm a}^{-1}$  to  $210 \text{ mm a}^{-1}$  at the respective

410 elevation. Assessing the actual amount fog drip for grass species like *Setaria sphacelata*  
411 under natural conditions is challenging and has so far not been accounted for.

412 In case that further discrimination below the surface would substantially alter the isotope  
413 signature, the bias would change continuously with depth. Any subsurface flow reaching wick  
414 samplers at lower elevations would then further increase the bias. However, the negative bias  
415 of  $-16.19 (\pm 2.80 \text{ SD}) \text{ ‰ } \delta^2\text{H}$  in all monitored top wick samplers during validation accounts  
416 for most of the observed bias in the two deeper wick samplers amounting to  
417  $-17.32 (\pm 2.47 \text{ SD}) \text{ ‰ } \delta^2\text{H}$ . Thus we conclude that the bias is mainly a result of constraints  
418 related to modeling surface processes, rather than subsurface ones.

419 Figure 4 shows the behavior of the chosen parameter sets for saturated hydraulic conductivity  
420 and groundwater depth during calibration and validation. The parameter space allows us to  
421 assess the range of suitable parameters and their sensitivity over a given parameter range.  
422 During calibration the given parameter space could not be constrained to more precise values  
423 for all parameters, which in this case should show a lower SD (Tab. 6) and narrower box plots  
424 (Figure 4). Especially the  $K_{\text{sat}}$  values of the soil layers A1, A3 and B1-B3, the porosity for all  
425 soil layers (not included in Figure 4) and the groundwater depth depict a low sensitivity over  
426 the entire calibration range (indicated by a high SD, wide box plot, and evenly scattered  
427 points; Tab. 6 and Figure 4). In particular the low sensitivity of the model towards  
428 groundwater depth seems surprising, but can be explained by the potentially low saturated  
429 hydraulic conductivities of the lower soil layers C1 and C2 limiting the percolation into the  
430 lower soil layers outside of the modeling domain. Even an extreme hydraulic potential,  
431 induced by a deep groundwater body, can be limited by a low hydraulic conductivity. None  
432 the less it noteworthy, that no model run without an active groundwater body as a lower  
433 boundary condition (groundwater depth < 2 m) results in a model performance with  $\text{NSE} > 0$   
434 (Figure 4). With a groundwater depth above 2 m the boundary condition would serve as a

435 source of water with an undefined isotopic signal and prevent any percolation of water into  
436 deeper soil layers outside of the modeling domain. The results are therefore in alignment with  
437 the topography of the system indicating an active groundwater body deeper than 2 m and  
438 support our second hypothesis which we will further discuss in section 3.2. We identified  
439 several parameter combinations showing the same model performance, known as equifinality  
440 according to Beven and Freer (2001). The observed equifinality can partially be explained by  
441 counteracting effects of a decreasing  $K_{sat}$  and an increasing pore space, or that the water flow  
442 is restrained due to lower hydraulic conductivities at adjoining soil layers. Especially for  
443 deeper soil layers the interaction between surrounding layers makes it especially difficult to  
444 further constrain the given parameter range. Even though the parameter ranges for all  
445 behavioral model realizations are not so well confined, the small confidence intervals indicate  
446 a certain degree of robustness towards the predicted flows (Figure 3). Additional soil moisture  
447 measurements complementing the current setup in the future will allow us to put further  
448 confidence in this new approach and the drawn conclusions and allow us to directly compare  
449 different calibration targets (i.e. soil moisture vs. soil water isotopic signature).

450 Initial  $K_{sat}$  values based on literature values (see Tab. 1) deviate to a large extent from those  
451 derived through the calibration process. This is attributable to the occurrence of preferential  
452 flow within the macro pores (Bronstert and Plate, 1997) and the sampling method (PCaps)  
453 used to extract the soil water stored in the soil with a matrix potential up to 30 hPa (Landon et  
454 al., 1999). It becomes apparent that the mixing processes (based on dispersion and molecular  
455 diffusion) are not sufficient to equilibrate the isotope signature over the entire pore space  
456 (Landon et al., 1999; Šimůnek et al., 2003) and that the flow through the pore space is not  
457 homogenous. Thus the isotopic signature between the sampled pore media and the total  
458 modeled pore space differs (Brooks et al., 2010; Hrachowitz et al., 2013; McDonnell and  
459 Beven, 2014; McGlynn et al., 2002). The model tries to account for these effects by favoring  
460 high  $K_{sat}$  values during calibration (McDonnell and Beven, 2014; McGlynn et al., 2002).

461 Modeling soil water movement under such conditions should therefore be used with caution  
462 for models based on Darcy-Richards equation which assume instantaneously homogeneous  
463 mixed solutions and uniform flow. In line with the argumentation started by Beven and  
464 Germann (1982) and refreshed in their recent paper Beven and Germann (2013) we therefore  
465 stress the importance to account for preferential flow processes and overcome the limitation  
466 of Darcy-Richards equation limiting the explanatory power of hydrological models predicting  
467 water flow and solute/isotope transport in particular. Like Gerke (2006) and Šimůnek and van  
468 Genuchten (2008) among others we therefore seek to implement a dual permeability approach  
469 accounting for different flow patterns within the soil pore space (Gerke, 2006; Jarvis, 2007;  
470 Šimůnek and van Genuchten, 2008; Vogel et al., 2000, 2006, 2010). In the style of existing 1-  
471 Dmodels for soil water isotope transport presented by Braud et al. (2005) and Haverd and  
472 Cuntz (2010) the inter-soil mixing processes by dispersion and molecular diffusion between  
473 different soil pore space compartments shall be accounted for in the future. Based on the  
474 presented findings this can now be extended towards the development and application of soil  
475 water isotope models under natural conditions. To conclude, the results highlight the general  
476 suitability of high resolution soil water isotope profiles to improve our understanding of  
477 subsurface water flux separation implemented in current hillslope model applications and to  
478 predict subsurface soil water movement.

### 479 **3.2 Modeled water fluxes**

480 Acknowledging the general suitability of the model to delineate the prevailing flow patterns,  
481 we will now compare those to the current hydrological process understanding presented in the  
482 introduction. Figure 5 depicts the water balance of the modeled hillslope based on all  
483 behavioral model realizations, separating the amount of incoming precipitation into the main  
484 flow components: surface runoff and subsurface flow directly entering the stream, percolation  
485 to groundwater and evapotranspiration.

486 Evapotranspiration is further subdivided into transpiration and evaporation from the soil  
487 surface and the canopy, whereby evaporation from the canopy is designated as interception  
488 losses. Due to the small confidence intervals of the behavioral model runs (see Figure 3) the  
489 standard deviations of the model's flow components are relatively small (see Figure 5;  
490 standard deviation and mean value was computed without weighting the likelihood value).

491 The observed order of magnitude for evapotranspiration is in good agreement with previous  
492 values of 945 and 876 mm a<sup>-1</sup> reported for tropical grasslands by Windhorst et al. (2013a) and  
493 Oke (1987), respectively. As previously mentioned the evaporation of 382 mm a<sup>-1</sup> is  
494 dominated by interception losses accounting for 344 mm a<sup>-1</sup>. Overall, these results support  
495 hypothesis II, which stated that a large share of the incoming precipitation is routed through  
496 the deeper soil layer and/or the groundwater body (here 49.7% or 942 mm a<sup>-1</sup>) before it enters  
497 the stream. This also explains the long mean transit time of water of around 1.0 to 3.9 years  
498 (Crespo et al., 2012; Timbe et al., 2014) in comparison to the fast runoff reaction time. Well  
499 in agreement with our current process understanding and hypothesis III, we can further show  
500 that the occurrence of surface runoff (33 mm a<sup>-1</sup>) due to Hortonian overland flow is less  
501 important. For the graphical representation the surface runoff has therefore been combined  
502 with subsurface flow (2 mm a<sup>-1</sup>) to "surface runoff & subsurface flow", accounting in total for  
503 35 mm a<sup>-1</sup> (see Figure 5). A more heterogeneous picture can be depicted if we take a closer  
504 look at the flow processes along the studied hillslope and its soil profiles (Figure 6).

505 Vertical fluxes still dominate the flow of water (Figure 6b), but the near surface lateral flow  
506 components predicted by Bückner et al. (2010) become more evident (Figure 6a). Explained by  
507 the high saturated hydraulic conductivities in the top soil layers (Tab. 6 and Figure 4) up to  
508  $7.3 \cdot 10^3 \text{ m}^3 \text{ a}^{-1}$  are transported lateral between cells in the top soil layer, referring to 15.6% of  
509 the total flow leaving the system per year. According to the model results deep lateral flow is  
510 minimal accounting only for <0.1% of the total flow. It only occurs on top of the deeper soil

511 horizons with low  $K_{\text{sat}}$  values. For all behavioral model realizations the groundwater level was  
512  $>2$  m thereby limiting the direct contribution of subsurface flow ( $2 \text{ mm a}^{-1}$ ) to the tributary,  
513 which had a hydraulic potential of only 1.5 m. Over the entire hillslope the importance of  
514 overland flow remains below 3% ( $\approx 50 \text{ mm a}^{-1}$ ), of which a part is re-infiltrating, summing up  
515 to total overland flow losses of around 2% at the hillslope scale ( $35 \text{ mm a}^{-1}$ , Figure 5). These  
516 results demonstrate the importance of near surface lateral flow and hence support hypothesis  
517 IV.

#### 518 **4 Conclusion**

519 These data and findings support and complement the existing process understanding mainly  
520 gained by Goller et al. (2005), Fleischbein et al. (2006) Boy et al. (2008), Bücken et al.  
521 (2010), Crespo et al. (2012) and Timbe et al. (2014) to a large extend. Moreover, it was  
522 possible to quantify for the first time the relevance of near surface lateral flow generation. The  
523 observed dominance of vertical percolation into the groundwater body and thereby the  
524 importance of preferential flow seems to be quite common for humid tropical montane  
525 regions and has recently been reported by Muñoz-Villers & McDonnell (2012) in a similar  
526 environment.

527 Being aware of the rapid rainfall-runoff response of streams within the catchment of the Rio  
528 San Francisco it has been questioned whether and how the system can store water for several  
529 years and still release it within minutes. Throughout the last decades several studies have  
530 observed similar hydrological behavior especially for steep humid montane regions (e.g.  
531 McDonnell (1990) and Muñoz-Villers & McDonnell (2012)) and concepts have been  
532 developed to explain this behavior: e.g. piston flow (McDonnell, 1990), kinematic waves  
533 (Lighthill and Whitham, 1955), transmissivity feedback (Kendall et al., 1999). Due to the  
534 limited depth of observations (max. depth 0.4 m) and the low overall influence of the lateral  
535 flows a more exact evaluation of the fate of the percolated water is still not possible.

536 However, we are confident, that in combination with a suitable concept to account for the  
537 rapid mobilization of the percolated water into a tributary and experimental findings, further  
538 confining possible model realizations an improved version of the current approach, could  
539 further close the gap in our current process understanding.

540 Over decades hydrological models which are based on the Richards or Darcy equation (like  
541 the one we used), have been tuned to predict quantitative flow processes and mostly been  
542 validated using soil moisture data suitable to account for overall storage changes. Our results  
543 imply that doing this considerably well does not necessarily mean that the models actually  
544 transport the *right* water at the *right* time. Using tracer data to validate models as we did  
545 entails that those models now not only have to transport the correct amount but additionally  
546 the *right* water. Consequently, the relevance of the correct representation of uneven  
547 preferential flow through pipes or macropores, which is misleadingly compensated by high  
548 conductivities over the entire pore space within models based on the Richards or Darcy  
549 equation, becomes immense. Distinguishing between water flowing in different compartments  
550 (e.g. pipes, cracks and macro pores) of the soil is a key task to get a closer and more precise  
551 representation of the natural flow processes. Even though the chosen modeling structure  
552 currently lacks a sufficient robustness to be widely applicable it highlights the potential and  
553 future research directions for soil water isotope modeling.

554 **Acknowledgments**

555  
556 The current study was conducted within the DFG Research Group FOR 816 “Biodiversity and  
557 sustainable management of a megadiverse mountain rain forest in south Ecuador” and the  
558 follow-up project PAK 825/3. The authors are very grateful for the funding supplied by the  
559 German Research Foundation DFG (BR2238/4-2 and BR 2238/14-1) and thank Thorsten  
560 Peters of the University of Erlangen for providing meteorological data.

561

562 **References**

- 563 Barthold, F.K., Tyralla, C., Schneider, K., Vaché, K.B., Frede, H.-G., Breuer, L., 2011. How  
564 many tracers do we need for end member mixing analysis (EMMA)? A sensitivity  
565 analysis. *Water Resour. Res.* 47, W08519. doi:10.1029/2011WR010604
- 566 Beck, E., Makeschin, F., Haubrich, F., Richter, M., Bendix, J., Valerezo, C., 2008. The  
567 Ecosystem (Reserva Biológica San Francisco), in: Beck, E., Bendix, J., Kottke, I.,  
568 Makeschin, F., Mosandl, R. (Eds.), *Gradients in a Tropical Mountain Ecosystem of*  
569 *Ecuador, Ecological Studies.* Springer Berlin Heidelberg, pp. 1–13.
- 570 Bendix, J., Rollenbeck, R., Richter, M., Fabian, P., Emck, P., 2008. Climate, in: Beck, E.,  
571 Bendix, J., Kottke, I., Makeschin, F., Mosandl, R. (Eds.), *Gradients in a Tropical*  
572 *Mountain Ecosystem of Ecuador, Ecological Studies.* Springer Berlin Heidelberg, pp.  
573 63–73.
- 574 Bendix, J., Silva, B., Roos, K., Göttlicher, D.O., Rollenbeck, R., Nauß, T., Beck, E., 2010.  
575 Model parameterization to simulate and compare the PAR absorption potential of two  
576 competing plant species. *Int. J. Biometeorol.* 54, 283–295. doi:10.1007/s00484-009-  
577 0279-3
- 578 Beven, K., Germann, P., 1982. Macropores and water flow in soils. *Water Resour. Res.* 18,  
579 1311–1325. doi:10.1029/WR018i005p01311
- 580 Beven, K., Germann, P., 2013. Macropores and water flow in soils revisited. *Water Resour.*  
581 *Res.* 49, 3071–3092. doi:10.1002/wrcr.20156
- 582 Bogner, C., Bauer, F., Trancón y Widemann, B., Viñan, P., Balcazar, L., Huwe, B., 2014.  
583 Quantifying the morphology of flow patterns in landslide-affected and unaffected  
584 soils. *J. Hydrol.* 511, 460–473. doi:10.1016/j.jhydrol.2014.01.063
- 585 Boy, J., Valerezo, C., Wilcke, W., 2008. Water flow paths in soil control element exports in  
586 an Andean tropical montane forest. *Eur. J. Soil Sci.* 59, 1209–1227.  
587 doi:10.1111/j.1365-2389.2008.01063.x
- 588 Braud, I., Bariac, T., Gaudet, J.P., Vauclin, M., 2005. SiSPAT-Isotope, a coupled heat, water  
589 and stable isotope (HDO and H218O) transport model for bare soil. Part I. Model  
590 description and first verifications. *J. Hydrol.* 309, 277–300.  
591 doi:10.1016/j.jhydrol.2004.12.013
- 592 Bronstert, A., 1999. Capabilities and limitations of detailed hillslope hydrological modelling.  
593 *Hydrol. Process.* 13, 21–48. doi:10.1002/(SICI)1099-1085(199901)13:1<21::AID-  
594 HYP702>3.0.CO;2-4

- 595 Bronstert, A., Plate, E.J., 1997. Modelling of runoff generation and soil moisture dynamics for  
596 hillslopes and micro-catchments. *J. Hydrol.* 198, 177–195. doi:10.1016/S0022-  
597 1694(96)03306-9
- 598 Brooks, J.R., Barnard, H.R., Coulombe, R., McDonnell, J.J., 2010. Ecohydrologic separation  
599 of water between trees and streams in a Mediterranean climate. *Nat. Geosci.* 3, 100–  
600 104. doi:10.1038/ngeo722
- 601 Bücker, A., Crespo, P., Frede, H.-G., Breuer, L., 2011. Solute behaviour and export rates in  
602 neotropical montane catchments under different land-uses. *J. Trop. Ecol.* 27, 305–317.  
603 doi:10.1017/S0266467410000787
- 604 Bücker, A., Crespo, P., Frede, H.-G., Vaché, K., Cisneros, F., Breuer, L., 2010. Identifying  
605 Controls on Water Chemistry of Tropical Cloud Forest Catchments: Combining  
606 Descriptive Approaches and Multivariate Analysis. *Aquat. Geochem.* 16, 127–149.  
607 doi:10.1007/s10498-009-9073-4
- 608 Colman, R.L., Wilson, G.P.M., 1960. The Effect of Floods on Pasture Plants. *Agric. Gaz.*  
609 NSW 71, 337–347.
- 610 Craig, H., 1961. Standard for Reporting Concentrations of Deuterium and Oxygen-18 in  
611 Natural Waters. *Science* 133, 1833–1834. doi:10.1126/science.133.3467.1833
- 612 Craig, H., Gordon, L.I., 1965. Deuterium and oxygen 18 variations in the ocean and the  
613 marine atmosphere, in: Tongiogi, E. (Ed.), *Proceedings of the Conference on the*  
614 *Stable Isotopes in Oceanographic Studies and Paleotemperatures.* Lishi e F., Pisa,  
615 Spoleto, Italy, pp. 9–130.
- 616 Crespo, P., Bücker, A., Feyen, J., Vaché, K.B., Frede, H.-G., Breuer, L., 2012. Preliminary  
617 evaluation of the runoff processes in a remote montane cloud forest basin using  
618 Mixing Model Analysis and Mean Transit Time. *Hydrol. Process.* 26, 3896–3910.  
619 doi:10.1002/hyp.8382
- 620 Davies, J., Beven, K., Rodhe, A., Nyberg, L., Bishop, K., 2013. Integrated modeling of flow  
621 and residence times at the catchment scale with multiple interacting pathways. *Water*  
622 *Resour. Res.* 49, 4738–4750. doi:10.1002/wrcr.20377
- 623 Dohnal, M., Vogel, T., Šanda, M., Jelínková, V., 2012. Uncertainty Analysis of a Dual-  
624 Continuum Model Used to Simulate Subsurface Hillslope Runoff Involving Oxygen-  
625 18 as Natural Tracer. *J. Hydrol. Hydromech.* 60, 194–205. doi:10.2478/v10098-012-  
626 0017-0
- 627 Dubbert, M., Cuntz, M., Piayda, A., Maguás, C., Werner, C., 2013. Partitioning  
628 evapotranspiration – Testing the Craig and Gordon model with field measurements of  
629 oxygen isotope ratios of evaporative fluxes. *J. Hydrol.* 496, 142–153.  
630 doi:10.1016/j.jhydrol.2013.05.033
- 631 Federer, C.A., Vörösmarty, C., Fekete, B., 2003. Sensitivity of Annual Evaporation to Soil  
632 and Root Properties in Two Models of Contrasting Complexity. *J. Hydrometeorol.* 4,  
633 1276–1290. doi:10.1175/1525-7541(2003)004<1276:SOAETS>2.0.CO;2
- 634 Fleischbein, K., Wilcke, W., Valarezo, C., Zech, W., Knoblich, K., 2006. Water budgets of  
635 three small catchments under montane forest in Ecuador: experimental and modelling  
636 approach. *Hydrol. Process.* 20, 2491–2507. doi:10.1002/hyp.6212
- 637 Frisbee, M.D., Phillips, F.M., Campbell, A.R., Hendrickx, J.M.H., 2010. Modified passive  
638 capillary samplers for collecting samples of snowmelt infiltration for stable isotope  
639 analysis in remote, seasonally inaccessible watersheds 1: laboratory evaluation.  
640 *Hydrol. Process.* 24, 825–833. doi:10.1002/hyp.7523
- 641 Garvelmann, J., Külls, C., Weiler, M., 2012. A porewater-based stable isotope approach for  
642 the investigation of subsurface hydrological processes. *Hydrol Earth Syst Sci* 16, 631–  
643 640. doi:10.5194/hess-16-631-2012

644 Genereux, D.P., Hooper, R.P., 1999. Oxygen and hydrogen isotopes in rainfall-runoff studies,  
645 in: Kendall, C., McDonnell, J.J. (Eds.), *Isotope Tracers in Catchment Hydrology*.  
646 Elsevier, pp. 319–346.

647 Gerke, H.H., 2006. Preferential flow descriptions for structured soils. *J. Plant Nutr. Soil Sci.*  
648 169, 382–400. doi:10.1002/jpln.200521955

649 Germann, P., Helbling, A., Vadilonga, T., 2007. Rivulet Approach to Rates of Preferential  
650 Infiltration. *Vadose Zone J.* 6, 207. doi:10.2136/vzj2006.0115

651 Goller, R., Wilcke, W., Leng, M.J., Tobschall, H.J., Wagner, K., Valarezo, C., Zech, W.,  
652 2005. Tracing water paths through small catchments under a tropical montane rain  
653 forest in south Ecuador by an oxygen isotope approach. *J. Hydrol.* 308, 67–80.  
654 doi:10.1016/j.jhydrol.2004.10.022

655 Hacker, J.B., Jones, R.J., 1969. The *Setaria sphacelata* complex - a review. *Trop. Grassl.* 3,  
656 13–34.

657 Haverd, V., Cuntz, M., 2010. Soil–Litter–Iso: A one-dimensional model for coupled transport  
658 of heat, water and stable isotopes in soil with a litter layer and root extraction. *J.*  
659 *Hydrol.* 388, 438–455. doi:10.1016/j.jhydrol.2010.05.029

660 Hrachowitz, M., Savenije, H., Bogaard, T.A., Tetzlaff, D., Soulsby, C., 2013. What can flux  
661 tracking teach us about water age distribution patterns and their temporal dynamics?  
662 *Hydrol Earth Syst Sci* 17, 533–564. doi:10.5194/hess-17-533-2013

663 Hsieh, J.C., Chadwick, O.A., Kelly, E.F., Savin, S.M., 1998. Oxygen isotopic composition of  
664 soil water: Quantifying evaporation and transpiration. *Geoderma* 82, 269–293.  
665 doi:10.1016/S0016-7061(97)00105-5

666 Hunter, J.D., 2007. Matplotlib: A 2D Graphics Environment. *Comput. Sci. Eng.* 9, 90–95.  
667 doi:10.1109/MCSE.2007.55

668 Huwe, B., Zimmermann, B., Zeilinger, J., Quizhpe, M., Elsenbeer, H., 2008. Gradients and  
669 Patterns of Soil Physical Parameters at Local, Field and Catchment Scales, in: Beck,  
670 E., Bendix, J., Kottke, I., Makeschin, F., Mosandl, R. (Eds.), *Gradients in a Tropical*  
671 *Mountain Ecosystem of Ecuador*, Ecological Studies. Springer Berlin Heidelberg, pp.  
672 375–386.

673 Jarvis, N.J., 2007. A review of non-equilibrium water flow and solute transport in soil  
674 macropores: principles, controlling factors and consequences for water quality. *Eur. J.*  
675 *Soil Sci.* 58, 523–546. doi:10.1111/j.1365-2389.2007.00915.x

676 Kendall, K.A., Shanley, J.B., McDonnell, J.J., 1999. A hydrometric and geochemical  
677 approach to test the transmissivity feedback hypothesis during snowmelt. *J. Hydrol.*  
678 219, 188–205. doi:10.1016/S0022-1694(99)00059-1

679 Kirkby, M., 1988. Hillslope runoff processes and models. *J. Hydrol.* 100, 315–339.  
680 doi:10.1016/0022-1694(88)90190-4

681 Körner, C., Scheel, J., Bauer, H., 1979. Maximum leaf diffusive conductance in vascular  
682 plants. *Photosynthetica* 13, 45–82.

683 Kraft, P., Multsch, S., Vaché, K.B., Frede, H.-G., Breuer, L., 2010. Using Python as a  
684 coupling platform for integrated catchment models. *Adv. Geosci.* 27, 51–56.  
685 doi:10.5194/adgeo-27-51-2010

686 Kraft, P., Vaché, K.B., Frede, H.-G., Breuer, L., 2011. CMF: A Hydrological Programming  
687 Language Extension For Integrated Catchment Models. *Environ. Model. Softw.* 26,  
688 828–830. doi:10.1016/j.envsoft.2010.12.009

689 Landon, M.K., Delin, G.N., Komor, S.C., Regan, C.P., 1999. Comparison of the stable-  
690 isotopic composition of soil water collected from suction lysimeters, wick samplers,  
691 and cores in a sandy unsaturated zone. *J. Hydrol.* 224, 45–54. doi:10.1016/S0022-  
692 1694(99)00120-1

693 Leibundgut, C., Maloszewski, P., Külls, C., 2011. *Tracers in Hydrology*. John Wiley & Sons,  
694 Chichester, UK.

695 Lighthill, M.J., Whitham, G.B., 1955. On Kinematic Waves. II. A Theory of Traffic Flow on  
696 Long Crowded Roads. *Proc. R. Soc. Lond. Ser. Math. Phys. Sci.* 229, 317–345.  
697 doi:10.1098/rspa.1955.0089

698 Liu, W.J., Liu, W.Y., Li, P.J., Gao, L., Shen, Y.X., Wang, P.Y., Zhang, Y.P., Li, H.M., 2007.  
699 Using stable isotopes to determine sources of fog drip in a tropical seasonal rain forest  
700 of Xishuangbanna, SW China. *Agric. For. Meteorol.* 143, 80–91.  
701 doi:10.1016/j.agrformet.2006.11.009

702 McDonnell, J.J., 1990. A Rationale for Old Water Discharge Through Macropores in a Steep,  
703 Humid Catchment. *Water Resour. Res.* 26, 2821–2832.  
704 doi:10.1029/WR026i011p02821

705 McDonnell, J.J., Beven, K., 2014. Debates—The future of hydrological sciences: A  
706 (common) path forward? A call to action aimed at understanding velocities, celerities  
707 and residence time distributions of the headwater hydrograph. *Water Resour. Res.* 50,  
708 5342–5350. doi:10.1002/2013WR015141

709 McDonnell, J.J., Sivapalan, M., Vaché, K., Dunn, S., Grant, G., Haggerty, R., Hinz, C.,  
710 Hooper, R., Kirchner, J., Roderick, M.L., Selker, J., Weiler, M., 2007. Moving beyond  
711 heterogeneity and process complexity: A new vision for watershed hydrology. *Water*  
712 *Resour. Res.* 43, W07301. doi:10.1029/2006WR005467

713 McGlynn, B.L., McDonnell, J.J., Brammer, D.D., 2002. A review of the evolving perceptual  
714 model of hillslope flowpaths at the Maimai catchments, New Zealand. *J. Hydrol.* 257,  
715 1–26. doi:10.1016/S0022-1694(01)00559-5

716 McKay, M.D., Beckman, R.J., Conover, W.J., 1979. A Comparison of Three Methods for  
717 Selecting Values of Input Variables in the Analysis of Output from a Computer Code.  
718 *Technometrics* 21, 239–245. doi:10.2307/1268522

719 McMillan, H., Tetzlaff, D., Clark, M., Soulsby, C., 2012. Do time-variable tracers aid the  
720 evaluation of hydrological model structure? A multimodel approach. *Water Resour.*  
721 *Res.* 48, W05501. doi:10.1029/2011WR011688

722 Mertens, J., Diels, J., Feyen, J., Vanderborght, J., 2007. Numerical analysis of Passive  
723 Capillary Wick Samplers prior to field installation. *Soil Sci. Soc. Am. J.* 71, 35–42.  
724 doi:10.2136/sssaj2006.0106

725 Muñoz-Villers, L.E., McDonnell, J.J., 2012. Runoff generation in a steep, tropical montane  
726 cloud forest catchment on permeable volcanic substrate. *Water Resour. Res.* 48,  
727 W09528. doi:10.1029/2011WR011316

728 Oke, T.R., 1987. *Boundary Layer Climates*, 2nd ed. Methuen, London, UK.

729 Qu, Y., Duffy, C.J., 2007. A semidiscrete finite volume formulation for multiprocess  
730 watershed simulation. *Water Resour. Res.* 43, W08419. doi:10.1029/2006WR005752

731 Rhoades, C.C., Eckert, G.E., Coleman, D.C., 2000. Soil carbon differences among forest,  
732 agriculture, and secondary vegetation in lower montane Ecuador. *Ecol. Appl.* 10, 497–  
733 505. doi:10.1890/1051-0761(2000)010[0497:SCDAFA]2.0.CO;2

734 Scholl, M.A., Shanley, J.B., Zegarra, J.P., Coplen, T.B., 2009. The stable isotope amount  
735 effect: New insights from NEXRAD echo tops, Luquillo Mountains, Puerto Rico.  
736 *Water Resour. Res.* 45, W12407. doi:10.1029/2008WR007515

737 Shuttleworth, W.J., Gurney, R.J., 1990. The theoretical relationship between foliage  
738 temperature and canopy resistance in sparse crops. *Q. J. R. Meteorol. Soc.* 116, 497–  
739 519. doi:10.1002/qj.49711649213

740 Shuttleworth, W.J., Wallace, J.S., 1985. Evaporation from sparse crops—an energy  
741 combination theory. *Q. J. R. Meteorol. Soc.* 111, 839–855.  
742 doi:10.1002/qj.49711146910

743 Šimůnek, J., Jarvis, N.J., van Genuchten, M.T., Gärdenäs, A., 2003. Review and comparison  
744 of models for describing non-equilibrium and preferential flow and transport in the  
745 vadose zone. *J. Hydrol.* 272, 14–35. doi:10.1016/S0022-1694(02)00252-4

746 Šimůnek, J., van Genuchten, M.T., 2008. Modeling Nonequilibrium Flow and Transport  
747 Processes Using HYDRUS. *Vadose Zone J.* 7, 782–797. doi:10.2136/vzj2007.0074  
748 Sklash, M.G., Farvolden, R.N., Fritz, P., 1976. A conceptual model of watershed response to  
749 rainfall, developed through the use of oxygen-18 as a natural tracer. *Can. J. Earth Sci.*  
750 13, 271–283. doi:10.1139/e76-029  
751 Soulsby, C., Rodgers, P., Smart, R., Dawson, J., Dunn, S., 2003. A tracer-based assessment of  
752 hydrological pathways at different spatial scales in a mesoscale Scottish catchment.  
753 *Hydrol. Process.* 17, 759–777. doi:10.1002/hyp.1163  
754 Stumpff, C., Maloszewski, P., 2010. Quantification of preferential flow and flow  
755 heterogeneities in an unsaturated soil planted with different crops using the  
756 environmental isotope  $\delta^{18}\text{O}$ . *J. Hydrol.* 394, 407–415.  
757 doi:10.1016/j.jhydrol.2010.09.014  
758 Tetzlaff, D., McDonnell, J.J., Uhlenbrook, S., McGuire, K.J., Bogaart, P.W., Naef, F., Baird,  
759 A.J., Dunn, S.M., Soulsby, C., 2008. Conceptualizing catchment processes: simply too  
760 complex? *Hydrol. Process.* 22, 1727–1730. doi:10.1002/hyp.7069  
761 Thom, A.S., 1972. Momentum, mass and heat exchange of vegetation. *Q. J. R. Meteorol. Soc.*  
762 98, 124–134. doi:10.1002/qj.49709841510  
763 Timbe, E., Windhorst, D., Crespo, P., Frede, H.-G., Feyen, J., Breuer, L., 2014.  
764 Understanding uncertainties when inferring mean transit times of water trough tracer-  
765 based lumped-parameter models in Andean tropical montane cloud forest catchments.  
766 *Hydrol. Earth Syst. Sci.* 18, 1503–1523. doi:10.5194/hess-18-1503-2014  
767 Uhlenbrook, S., Roser, S., Tilch, N., 2004. Hydrological process representation at the meso-  
768 scale: the potential of a distributed, conceptual catchment model. *J. Hydrol.* 291, 278–  
769 296. doi:10.1016/j.jhydrol.2003.12.038  
770 Vogel, H.-J., Cousin, I., Ippisch, O., Bastian, P., 2006. The dominant role of structure for  
771 solute transport in soil: experimental evidence and modelling of structure and transport  
772 in a field experiment. *Hydrol Earth Syst Sci* 10, 495–506. doi:10.5194/hess-10-495-  
773 2006  
774 Vogel, T., Gerke, H.H., Zhang, R., Van Genuchten, M.T., 2000. Modeling flow and transport  
775 in a two-dimensional dual-permeability system with spatially variable hydraulic  
776 properties. *J. Hydrol.* 238, 78–89. doi:10.1016/S0022-1694(00)00327-9  
777 Vogel, T., Sanda, M., Dusek, J., Dohnal, M., Votrubova, J., 2010. Using Oxygen-18 to Study  
778 the Role of Preferential Flow in the Formation of Hillslope Runoff. *Vadose Zone J.* 9,  
779 252–259. doi:10.2136/vzj2009.0066  
780 Weiler, M., McDonnell, J., 2004. Virtual experiments: a new approach for improving process  
781 conceptualization in hillslope hydrology. *J. Hydrol.* 285, 3–18. doi:10.1016/S0022-  
782 1694(03)00271-3  
783 Wheeler, M.D., Newman, S.M., Orr-Ewing, A.J., Ashfold, M.N.R., 1998. Cavity ring-down  
784 spectroscopy. *J. Chem. Soc. Faraday Trans.* 94, 337–351. doi:10.1039/A707686J  
785 Windhorst, D., Brenner, S., Peters, T., Meyer, H., Thies, B., Bendix, J., Frede, H.-G., Breuer,  
786 L., 2013a. Impacts of Local Land-Use Change on Climate and Hydrology, in: Bendix,  
787 J., Beck, E., Bräuning, A., Makeschin, F., Mosandl, R., Scheu, S., Wilcke, W. (Eds.),  
788 Ecosystem Services, Biodiversity and Environmental Change in a Tropical Mountain  
789 Ecosystem of South Ecuador, *Ecological Studies* Vol. 221. Springer, Berlin,  
790 Heidelberg, New York, pp. 275–286.  
791 Windhorst, D., Waltz, T., Timbe, E., Frede, H.-G., Breuer, L., 2013b. Impact of elevation and  
792 weather patterns on the isotopic composition of precipitation in a tropical montane  
793 rainforest. *Hydrol. Earth Syst. Sci.* 17, 409–419. doi:10.5194/hess-17-409-2013  
794 Zimmermann, B., Elsenbeer, H., 2008. Spatial and temporal variability of soil saturated  
795 hydraulic conductivity in gradients of disturbance. *J. Hydrol.* 361, 78–95.  
796 doi:10.1016/j.jhydrol.2008.07.027

797 Zimmermann, U., Ehhalt, D., Muennich, K.O., 1968. Soil-Water Movement and  
798 Evapotranspiration: Changes in the Isotopic Composition of the Water., in: Isotopes in  
799 Hydrology. International Atomic Energy Agency, Vienna, pp. 567–585.  
800  
801

802 **Tables**803 **Tab. 1 Soil physical parameters**

Soil code	Clay [%]	Texture		Porosity [%]	$K_{sat}^*$ [m/d]	Van Genuchten- Mualem Parameters	
		Sand [%]	Silt [%]			$\alpha$	$n$
A1 & A1 top	34	17	49	81	0.324	0.641	1.16
A2 & A2 top	19	33	49	63	0.324	0.352	1.13
A3 & A3 top	15	34	51	74	0.324	0.221	1.24
B1	8	16	76	66	0.228	1.046	1.19
B2	15	34	51	59	0.228	0.145	1.13
B3	11	18	70	58	0.228	0.152	1.16
C1	15	45	40	55	0.026	0.023	1.12
C2	45	20	35	47	0.026	0.004	1.17

\* $K_{sat}$  values are based on values taken within the proximity of the hillslope under similar land use by Crespo et al. (2012) and Zimmermann and Elsenbeer (2008).

804

805 **Tab. 2 Plant (*Setaria sphacelata*) and soil dependent parameters used for the Shuttleworth-Wallace equation**

Parameter	Symbol	Value	Unit	Used to calculate	Source
<b>Potential soil surface resistance</b>	$r_{ss\ pot}$	500	$s\ m^{-1}$	$r_{ss}$	Federer et al.(2003)
<b>Max. stomatal conductivity or max. leaf conductance</b>	$g_{max}$	270	$s\ m^{-1}$	$r_{sc}$	Körner et al. (1979)
<b>Leaf area index</b>	LAI	3.7	$m^2\ m^{-2}$	$r_{sc}$	Bendix et al. (2010)
<b>Canopy height</b>	h	0.2	m	$r_{aa}, r_{ac}$ & $r_{as}$	Estimate based on hand measurements
<b>Representative leaf width</b>	w	0.015	m	$r_{ac}$	
<b>Extinction coefficient for photosynthetically active radiation in the canopy</b>	CR	70	%	$r_{sc}$	Federer et al.(2003)
<b>Canopy storage capacity</b>	-	0.15	$mm\ LAI^{-1}$	Interception	Federer et al.(2003)
<b>Canopy closure</b>	-	90	%	Throughfall	Estimate based on image evaluation
<b>Albedo</b>	alb	11,7	%	Net radiation	Bendix et al. (2010)

806

807

808 Tab. 3 Modeling periods

Description	Period		Duration [days]
	Start	End	
<b>Initial states</b>	1 July 2010	30 June 2012	730
<b>Warm up period</b>	1 July 2010	31 October 2010	122
<b>Calibration period</b>	1 November 2010	31 October 2011	364
<b>Validation period</b>	1 November 2011	31 October 2012	365

809

810 Tab. 4 Soil parameter ranges for the Monte Carlo simulations (assuming uniform distribution for each parameter).

Soil code	$K_{sat}$ [ $m\ d^{-1}$ ]		Porosity [ $m^3\ m^{-3}$ ]	
	Min.	Max.	Min.	Max.
A1-3 top	0.001	35	0.3	0.9
A1-3	0.001	30	0.3	0.9
B1-3	0.001	12	0.1	0.8
C1-2	0.001	8	0.1	0.8

811

812 Tab. 5 Model performance during calibration and validation for all behavioral model runs (based on all calibration  
813 runs with  $NSE > 0.15$ ,  $bias < \pm 20.0\%$   $\delta^2H$  and  $R^2 > 0.65$ ). Best modeled fit based on NSE.

	Calibration 2010-2011		Validation 2011-2012		Best modeled fit
	Mean	SD	Mean	SD	
<b>NSE</b>	0.19	0.008	0.35	0.029	0.42
<b>R<sup>2</sup></b>	0.67	0.008	0.66	0.020	0.84
<b>Bias</b>	-15.90	0.113	-16.93	0.344	-16.16

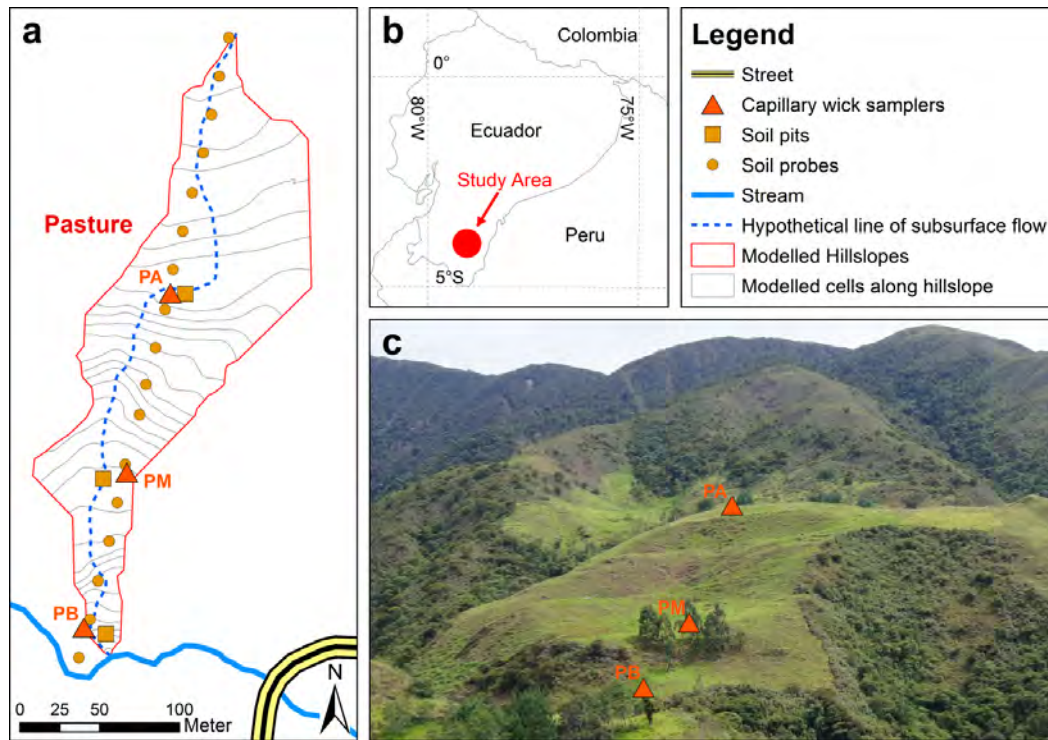
814

815  
816

**Tab. 6** Parameter ranges used for validation (all calibration runs with  $NSE > 0.15$ ,  $bias < \pm 20.0 \%$   $\delta^2H$  and  $R^2 > 0.65$ ) and parameter set for the best modeled fit based on NSE.

	Mean	SD	Best modeled fit
<b><math>K_{sat}</math> [<math>m\ d^{-1}</math>]</b>			
A1 top	21.8	5.8	20.4
A2 top	11.0	2.3	12.6
A3 top	25.6	6.3	29.6
A1	11.7	6.6	13.5
A2	7.4	2.8	8.9
A3	15.7	6.4	15.3
B1	4.0	2.4	4.0
B2	5.2	3.2	10.5
B3	4.6	2.2	2.5
C1	1.3	1.2	0.6
C2	1.7	1.4	0.1
<b>Porosity [<math>m^3\ m^{-3}</math>]</b>			
A1 top	0.54	0.08	0.44
A2 top	0.56	0.09	0.44
A3 top	0.66	0.09	0.53
A1	0.55	0.08	0.42
A2	0.55	0.09	0.46
A3	0.65	0.09	0.74
B1	0.34	0.09	0.31
B2	0.64	0.09	0.54
B3	0.75	0.09	0.70
C1	0.54	0.09	0.41
C2	0.55	0.09	0.67
<b>Groundwater depth [m]</b>			
	50.5	28.6	76.5

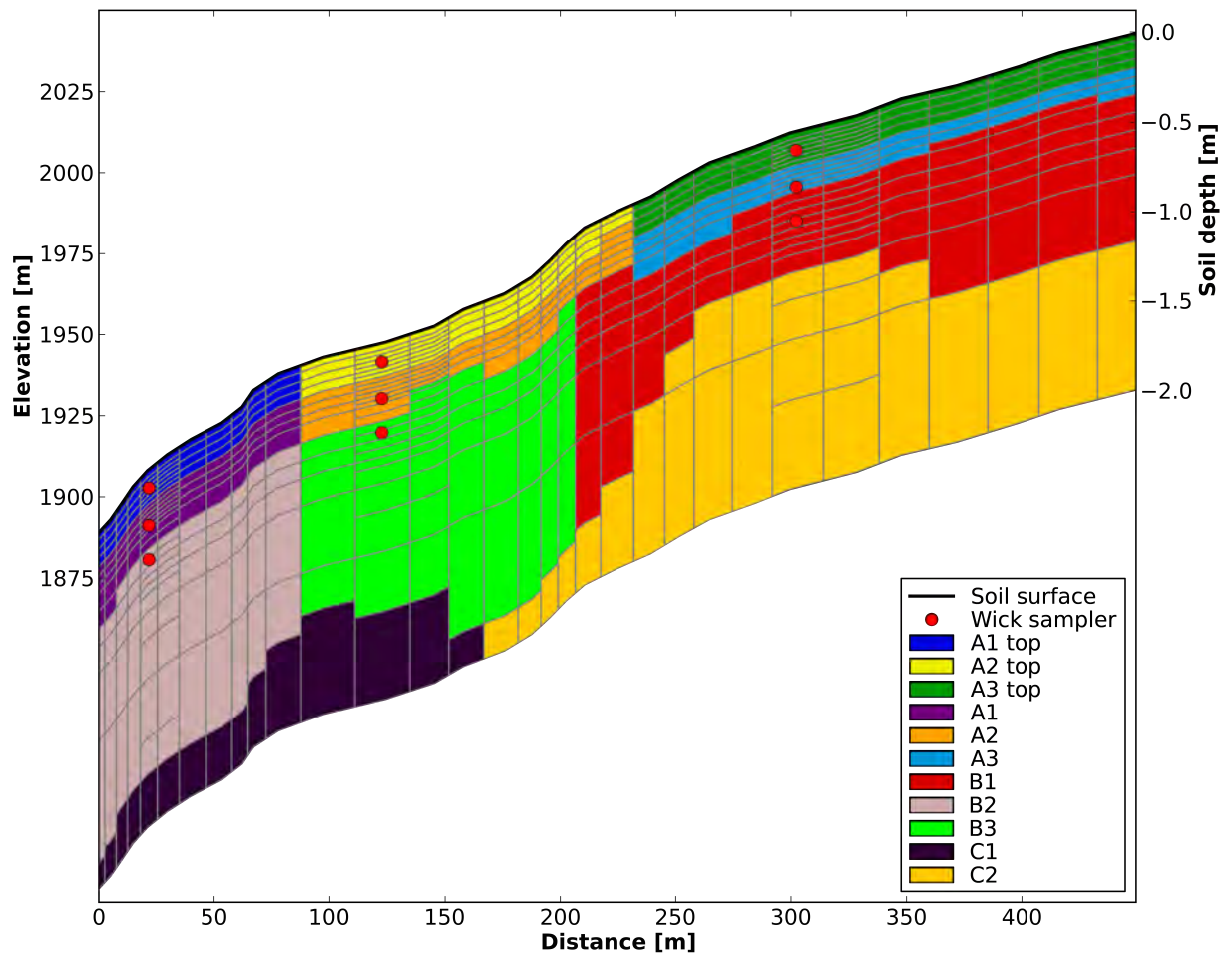
817



819

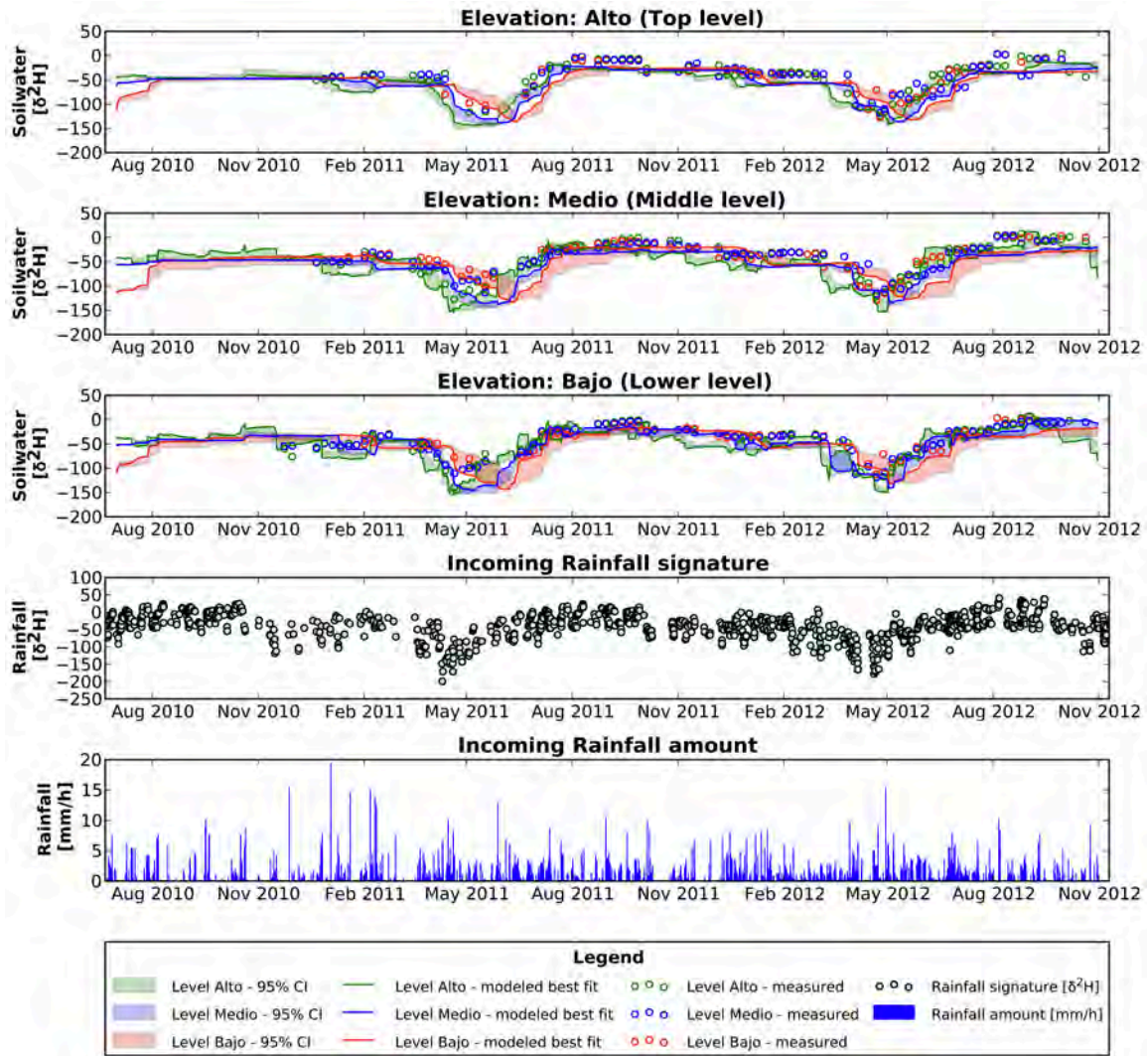
820 **Figure 1** a) Outline of the modeled hillslope and its virtual discretization into cells. b) Location of the study area  
 821 within Ecuador c) Photograph showing the Location of the wick samplers (P = Pasture and B = bajo/lower  
 822 level, M = medio/middle level, A = alto/top level sampler).

823



825 **Figure 2** Elevation profile (top black line, left ordinate), succession of soil layer types (color plate) and soil depths  
 826 assigned to the modeling grid (right ordinate).

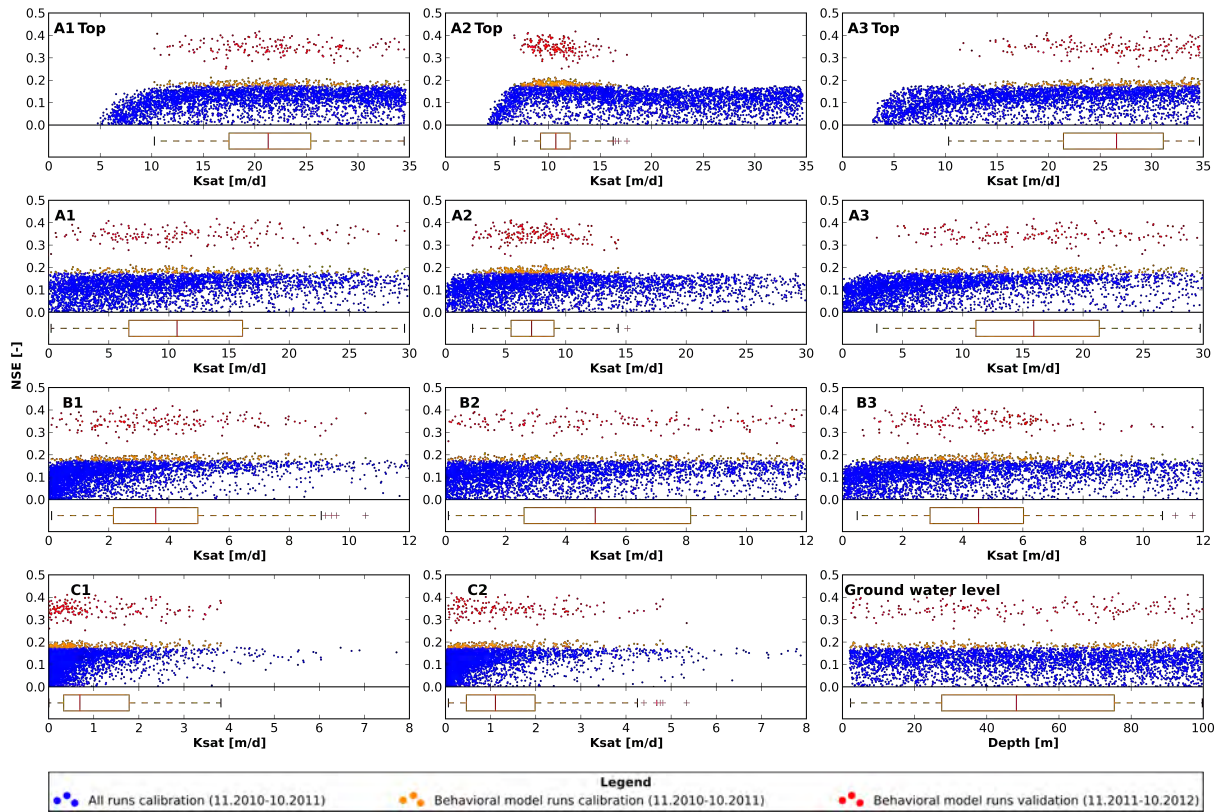
827



828

829 Figure 3 Time series of soil water isotope signatures (Top panels 1-3 for each elevation) for all behavioral model runs  
 830 with:  $NSE > 0.15$ ,  $bias < \pm 20.0 \text{‰ } \delta^2H$  and  $R^2 > 0.65$  showing the 95% confidence interval (CI; transparent  
 831 areas) and best modeled fit (solid line) vs. measured values (circles) at all 3 elevations (2,010, 1,949 and  
 832 1,904 m a.s.l.) and soil depths below ground (0.10, 0.25 and 0.40 m). Bottom panels 4 and 5, isotopic  
 833 signature and rainfall amount, respectively.

834

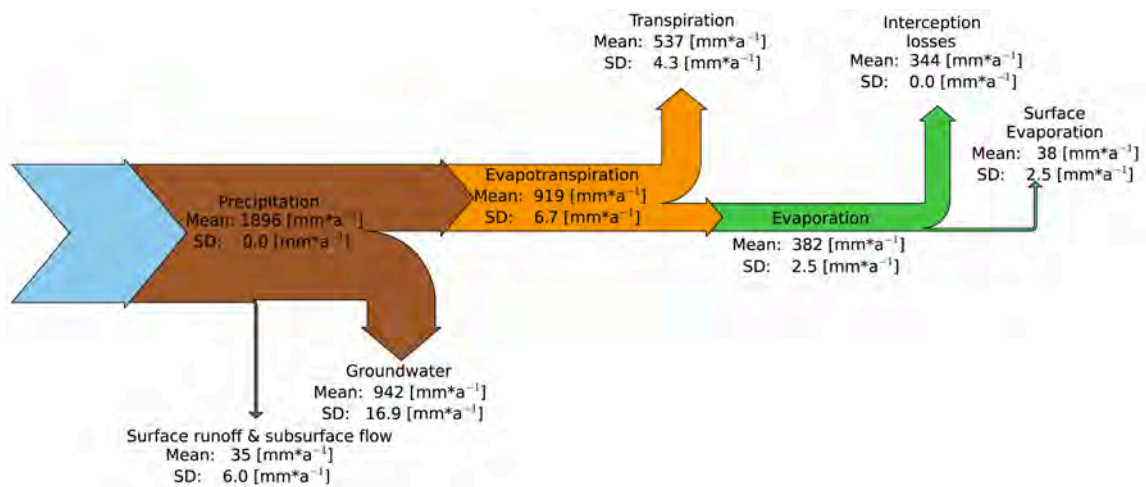


835

836 Figure 4 Dotty plots of NSE values (>0.0) during calibration (blue) and for behavioral model runs (NSE >0.15, bias  
 837 <±20.0 ‰ δ<sup>2</sup>H and R<sup>2</sup> > 0.65) during calibration (orange) and validation (red) for saturated hydraulic  
 838 conductivity (K<sub>sat</sub>) for all soil types and groundwater depth. Box plots show the unweighted parameter  
 839 distribution of all behavioral model runs (NSE > 0.15, bias < ± 20.0 ‰ δ<sup>2</sup>H and R<sup>2</sup> > 0.65). Results for soil  
 840 porosity look similar to those of the groundwater and are therefore not shown.

841

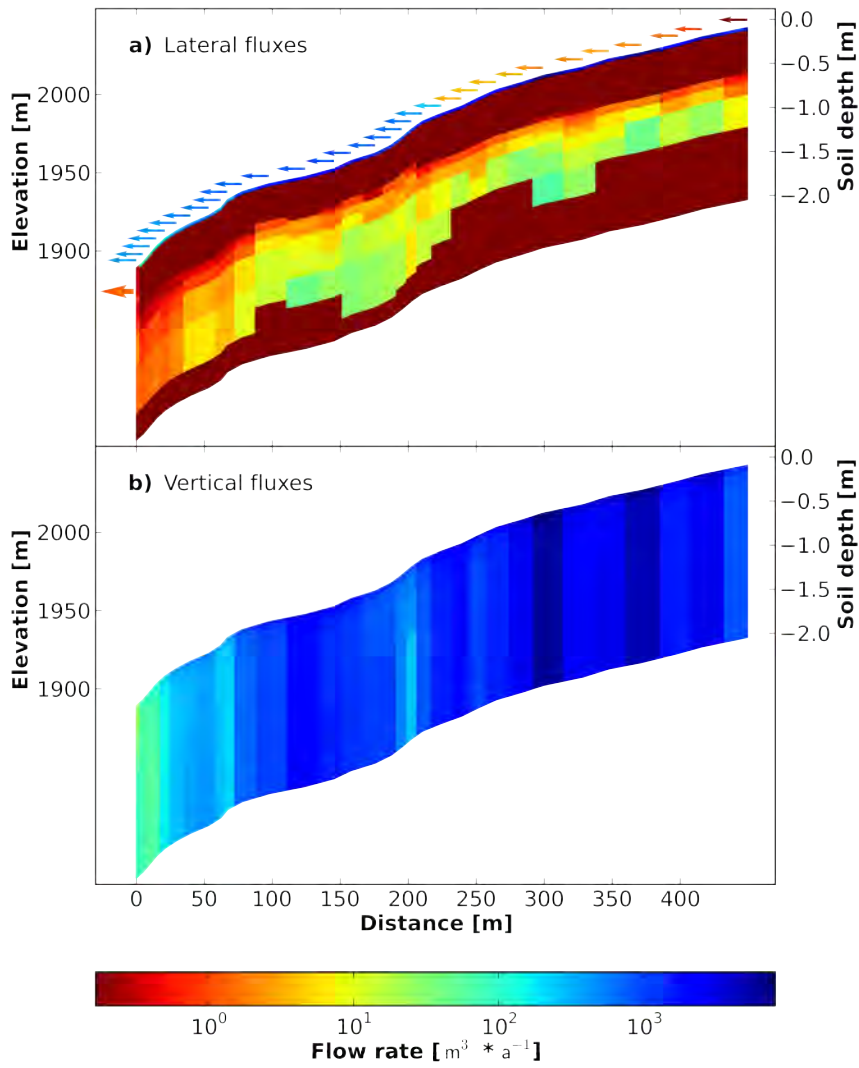
842



843

844 Figure 5 Mean annual flows and standard deviation (SD) of the main flow components at a hillslope scale of all  
 845 behavioral model runs from 2010-2012.

846



847

848 **Figure 6 a) Lateral and b) vertical fluxes for the best modeled fit. Arrows indicate the amount of surface runoff and**  
 849 **direct contribution to the outlet through subsurface flow. The maximum flow between storage compartments**  
 850 **is  $7.3 \cdot 10^3 \text{ m}^3 \text{ a}^{-1}$  and the total observed flow leaving as well as entering the system accumulates to  $37 \cdot 10^3 \text{ m}^3 \text{ a}^{-1}$ .**  
 851

852

Revised manuscript  
(showing changes)

1 **Stable water isotope tracing through hydrological models for**  
2 **disentangling runoff generation processes at the hillslope scale**

3

4 David Windhorst<sup>1</sup>, Philipp Kraft<sup>1</sup>, Edison Timbe<sup>1,2</sup>, Hans-Georg Frede<sup>1</sup>, Lutz Breuer<sup>1</sup>

5

6 [1] {Institute for Landscape Ecology and Resources Management (ILR), Research Centre for  
7 BioSystems, Land Use and Nutrition (IFZ), Justus-Liebig-Universität Gießen, Germany}

8 [2] {Grupo de Ciencias de la Tierra y del Ambiente, DIUC, Universidad de Cuenca,  
9 Ecuador}

10

11 Correspondence to: D. Windhorst ([david.windhorst@umwelt.uni-giessen.de](mailto:david.windhorst@umwelt.uni-giessen.de))

## 12 **Abstract**

13 Hillslopes are the dominant landscape components where incoming precipitation is  
14 transferred to become groundwater, streamflow or atmospheric water vapor. However,  
15 directly observing flux partitioning in the soil is almost impossible. Hydrological hillslope  
16 models are therefore being used to investigate the ~~involved~~ processes involved. Here we  
17 report on a modeling experiment using the Catchment Modeling Framework (CMF) where  
18 measured stable water isotopes in vertical soil profiles along a tropical mountainous grassland  
19 hillslope transect are traced through the model to resolve potential mixing processes. CMF  
20 simulates advective transport of stable water isotopes  $^{18}\text{O}$  and  $^2\text{H}$  based on the Richards  
21 equation within a fully distributed 2-D representation of the hillslope. The model successfully  
22 replicates the observed temporal pattern of soil water isotope profiles ( $R^2$  0.84 and NSE 0.42).  
23 Predicted flows are in good agreement with previous studies. We highlight the importance of  
24 groundwater recharge and shallow lateral subsurface flow, accounting for 50% and 16% of  
25 the total flow leaving the system, respectively. Surface runoff is negligible despite the steep  
26 slopes in the Ecuadorian study region.

27

## 28 **1 Introduction**

29 Delineating flow path in a hillslope is still a challenging task (Bronstert, 1999; McDonnell et  
30 al., 2007; Tetzlaff et al., 2008; Beven and Germann, 2013). Though a more complete  
31 understanding in the partitioning of incoming water to surface runoff, lateral subsurface flow  
32 components or percolation allows to better understand, for example, the impact of climate and  
33 land use change on hydrological processes. Models are often used to test different rainfall-  
34 runoff generation processes and the mixing of water in the soil (e.g. Kirkby, 1988; Weiler and  
35 McDonnell, 2004). Due to the prevailing measurement techniques and therefore the available

36 datasets it has become common practice to base the validation of modeled hillslope flow  
37 processes on quantitative data on storage change. In the simplest case, system wide storage  
38 changes are monitored by discharge and groundwater level measurements or, on more  
39 intensively instrumented hillslopes, the storage change of individual soil compartments is  
40 monitored by soil moisture sensors. In the typical ~~2-D~~ flow regime of a slope, such models  
41 bear the necessity not only to account for the vertical but also for the lateral movements of  
42 water within the soil (Bronstert, 1999). Quantitative data on storage change in this regard are  
43 only suitable to account for the actual change in soil water volume, but not to ~~verify~~ assess the  
44 source or flow direction. Knowing tracer compositions of relevant hydrological components  
45 along a hillslope allows to ~~predict the~~ account for mixing processes and thereby to ~~verify~~  
46 delineate the actual source of the incoming water. Over the years a number of artificial, e.g.  
47 fluorescence tracers like Uranine, and natural tracers, e.g. chloride or stable water isotopes,  
48 have emerged. While the application of the artificial tracers is rather limited in space and time  
49 (Leibundgut et al., 2011), the latter ones can be used over a wide range of scales (Barthold et  
50 al., 2011; Genereux and Hooper, 1999; Leibundgut et al., 2011; Muñoz-Villers and  
51 McDonnell, 2012; Soulsby et al., 2003). Stable water isotopes such as oxygen-18 ( $^{18}\text{O}$ ) and  
52 hydrogen-2 ( $^2\text{H}$ ) are integral parts of water molecules and consequently ideal tracers of water.  
53 Over the last decades isotope tracer studies have proven to provide reliable results on varying  
54 scales (chamber, plot, hillslope to catchment scale) and surface types (open water, bare soils,  
55 vegetated areas) to delineate or describe flow processes under field experimental or laboratory  
56 conditions (Garvelmann et al., 2012; Hsieh et al., 1998; Sklash et al., 1976; Vogel et al., 2010;  
57 Zimmermann et al., 1968).

58 Although the first 1d process orientated models to describe the dynamics of stable water  
59 isotope profiles for open water bodies (Craig and Gordon, 1965) and a bit later for soils  
60 (Zimmermann et al., 1968) have been developed as early as in the mid 1960~~'ies~~, fully  
61 distributed ~~2-D~~ to ~~3-D~~ hydrological tracer models benefitting from the additional

62 information to be gained by stable water isotopes are still in their early development stages  
63 (Davies et al., 2013) or use strong simplifications of the flow processes (e.g. TAC<sup>D</sup> using a  
64 kinematic wave approach; Uhlenbrook et al., 2004). This can be attributed to the high number  
65 of interwoven processes affecting the soil water isotope fluxes not only in the soil's liquid  
66 phase but also in its vapor phase. The more process based 1d models (Braud et al., 2005;  
67 Haverd and Cuntz, 2010) therefore simultaneously solve the heat balance and the mass  
68 balance simultaneously for the liquid and the vapor phase and are thereby describing the:

- 69 • convection and molecular diffusion in the liquid and vapor phase,
- 70 • equilibrium fractionation between liquid and vapor phase,
- 71 • fractionation due to evaporation, and
- 72 • non-fractionated flux due to percolation and transpiration.

73 | To obtain and compute the data required to apply these kind of models beyond the plot scale  
74 | is still challenging. However, due to emerging measuring techniques the availability of  
75 | sufficient data becomes currently more realistic. Increasing computational power and  
76 | especially the cavity ring-down spectroscopy (CRDS) - a precise and cost effective method to  
77 | analyze the signature of stable water isotopes (Wheeler et al., 1998) - promise progress.

78 | Hence, it is tempting to investigate the suitability of isotope tracers to delineate hydrological  
79 | flow paths using a more physical modeling approach. Recent research in this direction  
80 | includes the work of McMillan et al. (2012) and Hrachowitz et al. (2013) using chloride as a  
81 | tracer to study the fate of water in catchments in the Scottish Highlands. Even though some  
82 | processes affecting the soil water isotope transport are still represented in a simplified manner  
83 | or could be , due to their limited effect/importance of the respective process within the given  
84 | study site, omitted, this approach allows us to determine the potential of soil water isotope  
85 | modeling in catchment hydrology and highlight future need for research. Hence, it is tempting  
86 | to investigate the suitability of isotope tracers to delineate hydrological flow paths using a

~~constrained, more complex modeling approach. Constrained in the way, that relevant processes could either be omitted, due to limited effect/importance of the respective process, or easily be incorporated into an existing modeling framework. To verify and validate the hydrological processes and the inferred results of a 2d model setup using the Catchment Modeling Framework (CMF; Kraft et al., 2011), we choose a study site within a catchment for which already a principle process understanding about prevailing soil water flows existed.~~

This study is conducted in a 75 km<sup>2</sup> montane rain forest catchment in south Ecuador, the upper part of the Rio San Francisco, which has been under investigation since 2007 ([Bogner et al., 2014](#); [Boy et al., 2008](#); [Bücker et al., 2011](#); [Crespo et al., 2012](#); [Fleischbein et al., 2006](#); [Goller et al., 2005](#); [Timbe et al., 2014](#); [Windhorst et al., 2013b](#)). The findings of those studies (briefly synthesized in section 2.3) will a) ease the setup of chosen model, b) let us define suitable boundary conditions for the chosen modeling approach and c) serve as a reference for the delineated flow bath. The additional information from previous studies conducted in the study area, will therefore highlight the potential of this new model approach to delineate hydrological flow paths under natural conditions and support our preliminary hydrological process understanding retrieved from more classical methods conducted in the past.~~and for which a number of studies on forested micro catchments ( $\approx 0.1$  km<sup>2</sup>) are at hand . Studies on both scales identify the similar hydrological processes to be active within the study area, which shall be briefly described in the following section.~~

~~Studies on the micro scale ([Boy et al., 2008](#); [Goller et al., 2005](#)), supported by solute data and end member mixing analysis at the meso scale ([Bücker et al., 2011](#); [Crespo et al., 2012](#)), showed that under presaturated conditions of the mineral soil fast ‘organic horizon flow’ in forested catchments dominates during discharge events. Due to an abrupt change in saturated hydraulic conductivity ( $K_{\text{sat}}$ ) between the organic ( $38.9 \text{ m d}^{-1}$ ) and the near surface mineral layer ( $0.15 \text{ m d}^{-1}$ ) this ‘organic horizon flow’ can contribute up to 78% to the total discharge~~

112 ~~during storm events (Fleischbein et al., 2006; Goller et al., 2005). However, the overall~~  
113 ~~importance of this ‘organic horizon flow’ is still disputable, because the rainfall intensity~~  
114 ~~rarely gets close to such a high saturated hydraulic conductivity. In 95% of the measured~~  
115 ~~rainfall events between Jun 2010 and Oct 2012 the intensity was below  $0.1 \text{ m d}^{-1}$  ( $\approx 4.1 \text{ mm h}^{-1}$ )~~  
116 ~~and was therefore 15 times lower than the saturated hydraulic conductivity of the mineral~~  
117 ~~soil layer below the organic layer under forest vegetation and around 30 times lower than the~~  
118 ~~saturated hydraulic conductivity of the top soil under pasture vegetation (Zimmermann and~~  
119 ~~Elsenbeer, 2008; Crespo et al., 2012). The same conclusion holds true for the occurrence of~~  
120 ~~surface runoff due to infiltration access on pasture (lacking a significant organic layer). Solely~~  
121 ~~based on rainfall intensities surface runoff is therefore relatively unlikely to contribute to a~~  
122 ~~larger extend in rainfall runoff generation. When and to which extent a presaturated~~  
123 ~~subsurface would still trigger surface runoff on pastures therefore remains to be investigated.~~

124 ~~Bücker et al. (2010) and Timbe et al. (2014) could show that base flow on the other hand has~~  
125 ~~a rather large influence on the annual discharge volume across different land use types,~~  
126 ~~accounting for >70% and >85%, respectively. These findings are also supported by the long~~  
127 ~~mean transit time (MTT) of the base flow for different sub-catchments of the Rio San~~  
128 ~~Francisco, varying according to Timbe et al. (2014) between 2.1 and 3.9 years. Accordingly,~~  
129 ~~the current findings confirm that the base flow —originating from deeper mineral soil and~~  
130 ~~bedrock layers— is dominating the overall hydrological system in the study area (Crespo et al.,~~  
131 ~~2012; Goller et al., 2005). Apart from this dominating source of base flow, Bücker et al.~~  
132 ~~(2010) identified near surface lateral flow as a second component to be relevant for the~~  
133 ~~generation of base flow for pasture sites. Within this catchment we selected a hillslope with a~~  
134 distinct drainage area and nearly homogenous land-use and established an experimental  
135 sampling scheme to monitor the isotopic signatures of the soil water of three soil profiles  
136 using passive capillary fiberglass wick samplers (PCaps). Based on the proposed modeling  
137 approach a 2-D virtual hillslope representation of this hillslope was then implemented using

138 | the Catchment Modeling Framework (CMF; Kraft et al., 2011). Due to the necessity to mix  
139 | the flows in accordance to the observed soil water isotope signatures we are confident, that  
140 | the degree of certainty for the modeled flow path will be higher, than for conventional  
141 | modeling approaches relying solely on quantitative information to evaluate the modeled data.  
142 | Replacing the calibration target bears now the necessity to mix the right amount and signature  
143 | of any given flow component, whereas the quantitative change only relies on the actual  
144 | amount of water leaving or entering any given compartment. We will quantify the following  
145 | flow components to disentangle the runoff generation processes: surface runoff, lateral  
146 | subsurface flow in the vadose zone and percolation to groundwater. The lateral subsurface  
147 | flow will be further subdivided into near surface lateral flow and deep lateral flow.

148 | To validate the chosen modeling approach and assess our process understanding we tested the  
149 | following hypotheses:

- 150 | I. Under the given environmental conditions - high precipitation and humidity -  
151 | (Bendix et al., 2008) and full vegetation cover (Dohnal et al., 2012; Vogel et al.,  
152 | 2010) only non-fractionating and advective water transport of isotopes is relevant.  
153 | Gaseous advection and diffusive process in the gaseous as well as the liquid phase  
154 | and the enrichment due to evaporation are negligible; hence the stable water  
155 | isotopes behave like a conservative tracer.
- 156 | II. Large shares of the soil water percolate to deeper horizons, thereby creating long  
157 | mean transit times (MTT) (Crespo et al., 2012; Timbe et al., 2014).
- 158 | III. Due to the high saturated conductivities of the top soil layers the generation  
159 | occurrence of Hortonian overland flow ~~surface runoff~~ is unlikely to have an  
160 | important contribution to the observed flows (Crespo et al., 2012)

161 IV. Fast near surface lateral flow contributes essentially to downhill water flows and  
162 play a relevant role to understand the overall hydrological system (Bücker et al.,  
163 2010).

164

## 165 2 Materials and Methods

### 166 2.1 Study area

167 The hillslope under investigation is located within the catchment of the Rio San Francisco in  
168 South Ecuador (3°58'30"S, 79°4'25"W) at the eastern outskirts of the Andes and  
169 encompasses an area of 75 km<sup>2</sup>. Close to the continental divide the landscape generally  
170 follows a continuous eastward decline towards the lowlands of the Amazon basin (Figure 1b).  
171 Due to the high altitudes (1720-3155m a.s.l.), the deeply incised valleys (slopes are on  
172 average 25°-40° over the entire watershed), the low population density and the partly  
173 protected areas of the Podocarpus National Park, the human impact within the catchment is  
174 relatively low. The southern flanks of the Rio San Francisco are covered by an almost pristine  
175 tropical mountain cloud forest and lie mostly within the Podocarpus National Park. At lower  
176 elevations the northern flanks have mostly been cleared by natural or slash-and-burn fires  
177 during the last decades and are now partially used for extensive pasture (*Setaria sphacelata*  
178 Schumach.), reforestation sites (*Pinus patula*), are covered by shrubs or invasive weeds  
179 (especially tropical bracken fern; *Pteridium aquilinum* L.). The climate exhibits a strong  
180 altitudinal gradient creating relatively low temperatures and high rainfall amounts (15.3°C  
181 and 2000 mm a<sup>-1</sup> at 1960 m a.s.l. to 9.5°C and >6000 mm a<sup>-1</sup> at 3180 m a.s.l.) with the main  
182 rainy season in the austral winter (Bendix et al., 2008). A comprehensive description of the  
183 soils, climate, geology and land use has been presented by Beck et al. (2008), Bendix et al.  
184 (2008) and Huwe et al. (2008).

## 185 2.2 Experimental hillslope

186 To test our understanding of hydrological processes within the study area we choose a  
187 hillslope with a nearly homogenous land use (Figure 1). It is located on an extensive pasture  
188 site with low intensity grazing by cows and dominated by *Setaria sphacelata*. *Setaria*  
189 *sphacelata* is an introduced tropical C4 grass species that forms a dense tussock grassland  
190 with a thick surface root mat (Rhoades et al., 2000). This grass is accustomed to high annual  
191 rainfall intensities ( $>750 \text{ mm a}^{-1}$ ), has a low drought resistance and tolerates water logging to  
192 a greater extent than other tropical grass types (Colman and Wilson, 1960; Hacker and Jones,  
193 1969). The hillslope has a drainage area of  $0.025 \text{ km}^2$ , a hypothetical length of the subsurface  
194 flow of 451 m and an elevation gradient of 157 m with an average slope of  $19.2^\circ$ . The soil  
195 catena of the slope was recorded by Pürckhauer sampling and soil pits. To investigate the  
196 passage of water through the hillslope a series of three wick sampler has been installed along  
197 the line of subsurface flow.

198 Climate forcing data with an hourly resolution of precipitation, air temperature, irradiation,  
199 wind speed and relative humidity was collected by the nearby (400 m) climate station “ECSF”  
200 at similar elevation. Isotopic forcing data was collected manually for every rainfall event from  
201 Oct 2010 until Dec 2012 using a Ø25 cm funnel located in close proximity of the chosen  
202 hillslope at 1900 m a.s.l. (Timbe et al., 2014). To prevent any isotopic fractionation after the  
203 end of a single rainfall event (defined as a period of 30min without further rainfall) all  
204 samples were directly sealed with a lid and stored within a week in 2mL amber glass bottles  
205 for subsequent analysis of the isotopic signature as described in section 2.4.1 (all samples  
206 <2ml where discarded).

## 207 2.3 Current process understanding at the catchment scale

208 The catchment of the Rio San Francisco has been under investigation since 2007 (Bücker et  
209 al., 2011; Crespo et al., 2012; Timbe et al., 2014; Windhorst et al., 2013b) and was

210 complemented by a number of studies on forested micro catchments ( $\approx 0.1 \text{ km}^2$ ) within this  
211 catchment (Bogner et al., 2014; Boy et al., 2008; Fleischbein et al., 2006; Goller et al., 2005).  
212 Studies on both scales identify the similar hydrological processes to be active within the study  
213 area.

214 Studies on the micro scale (Boy et al., 2008; Goller et al., 2005), supported by solute data and  
215 end member mixing analysis at the meso scale (Bücker et al., 2011; Crespo et al., 2012),

216 showed that fast ‘organic horizon flow’ in forested catchments dominates during discharge  
217 events, if the mineral soils are water saturated prior to the rainfall.~~showed that under~~

218 ~~presaturated conditions of the mineral soil fast ‘organic horizon flow’ in forested catchments~~  
219 ~~dominates during discharge events.~~ Due to an abrupt change in saturated hydraulic

220 conductivity ( $K_{\text{sat}}$ ) between the organic ( $38.9 \text{ m d}^{-1}$ ) and the near-surface mineral layer  
221 ( $0.15 \text{ m d}^{-1}$ ) this ‘organic horizon flow’ can contribute up to 78% to the total discharge during

222 storm events (Fleischbein et al., 2006; Goller et al., 2005). However, the overall importance  
223 of this ‘organic horizon flow’ is still disputable, because the rainfall intensity rarely gets close

224 to such a high saturated hydraulic conductivity. In 95% of the measured rainfall events  
225 between Jun 2010 and Oct 2012 the intensity was below  $0.1 \text{ m d}^{-1}$  ( $\approx 4.1 \text{ mm h}^{-1}$ ) and was

226 therefore 15 times lower than the saturated hydraulic conductivity of the mineral soil layer  
227 below the organic layer under forest vegetation and around 30 times lower than the saturated

228 hydraulic conductivity of the top soil under pasture vegetation (Zimmermann and Elsenbeer,  
229 2008; Crespo et al., 2012). The same conclusion holds true for the occurrence of surface

230 runoff due to infiltration access on pasture (lacking a significant organic layer). Solely based  
231 on rainfall intensities surface runoff is therefore relatively unlikely to contribute to a larger

232 extend in rainfall-runoff generation. The reported  $K_{\text{sat}}$  values are based on measurements of  
233  $250 \text{ cm}^3$  undisturbed soil core samples vertically extracted from the center of each respective

234 layer. Due to the chosen sampling method and the limited size of the soil cores the effective

235 saturated hydraulic conductivity will be even higher and can vary for the horizontal flow  
236 component. When and to which extent a subsurface saturated prior the rainfall event  
237 ~~presaturated subsurface~~ would still trigger surface runoff on pastures therefore remains to be  
238 investigated.

239 Bücken et al. (2010) and Timbe et al. (2014) could show that base flow on the other hand has  
240 a rather large influence on the annual discharge volume across different land use types,  
241 accounting for >70% and >85%, respectively. These findings are also supported by the long  
242 mean transit time (MTT) of the base flow for different sub-catchments of the Rio San  
243 Francisco in comparison to the fast runoff reaction times, varying according to Timbe et al.  
244 (2014) between 2.1 and 3.9 years. Accordingly, the current findings confirm that the base  
245 flow – originating from deeper mineral soil and bedrock layers– is dominating the overall  
246 hydrological system in the study area (Crespo et al., 2012; Goller et al., 2005). Apart from this  
247 dominating source of base flow, Bücken et al. (2010) identified near surface lateral flow as a  
248 second component to be relevant for the generation of base flow for pasture sites.

## 249 **2.4 Measurements**

### 250 2.4.1 **Passive capillary fiberglass wick samplers (PCaps)**

251 We installed *passive capillary fiberglass wick samplers* (PCaps; short *wick samplers*,  
252 designed according to Mertens et al. (2007)) as soil water collectors at three locations along  
253 an altitudinal transects under pasture vegetation in three soil depths. PCaps maintain a fixed  
254 tension based on the type and length of wick (Mertens et al., 2007), require low maintenance  
255 and are most suitable to sample mobile soil water without altering its isotopic signature  
256 (Frisbee et al., 2010; Landon et al., 1999). We used woven and braided 3/8-inch fiberglass  
257 wicks (Amatex Co. Norristown, PA, US). 0.75 m of the 1.5 m wick was unraveled and placed  
258 over a 0.30 x 0.30 x 0.01 m square plastic plate, covered with fine grained parent soil material  
259 and then set in contact with the undisturbed soil.

260 Every collector was designed to sample water from three different soil depths (0.10, 0.25 and  
261 0.40 m) with the same suction, all having the same sampling area of 0.09 m<sup>2</sup>, wick type,  
262 hydraulic head of 0.3 m (vertical distance) and total wick length of 0.75 m. To simplify the  
263 collection of soil water the wick samplers drained into bottles placed inside a centralized tube  
264 with an inner diameter of 0.4 m and a depth of 1.0 m. To avoid any unnecessary alterations of  
265 the natural flow above the extraction area of the wick sampler the centralized tube was placed  
266 downhill and the plates were evenly spread uphill around the tube. A flexible silicon tube  
267 with a wall thickness of 5 mm was used to house the wick and to connect it to the 2 L  
268 sampling bottles storing the collected soil water. The silicon tube prevents evaporation and  
269 contamination of water flowing through the wick. Weekly bulk samples were collected over  
270 the period from Oct 2010 until Dec 2012 if the sample volume exceeded 2 mL. Soil water and  
271 the previously mentioned precipitation samples are ~~and~~ analyzed using a cavity ring down  
272 spectrometer (CRDS) with a precision of 0.1 per mil for <sup>18</sup>O and 0.5 for <sup>2</sup>H (Picarro L1102-i,  
273 CA, US).

#### 274 2.4.2 **Soil survey**

275 The basic soil and soil hydraulic properties for each distinct soil layer along the hillslope  
276 were investigated up to a depth of 2 m. Pürckhauer sampling for soil texture and succession  
277 of soil horizons was done every 25 m, while every 100 m soil pits were dug for sampling soil  
278 texture, soil water retention curves (pF-curves), porosity and succession of soil horizons. The  
279 results were grouped into 8 classes (Tab. 1) and assigned to the modeling mesh as shown in  
280 Figure 2. Retention curves (pF-curves) were represented by the *Van Genuchten-Mualem*  
281 function using the parameters  $\alpha$  and  $n$ .

282 All soils developed from the same parent material (clay schist) and are classified as Haplic  
283 Cambisol with varying soil thickness. Soil thickness generally increased downhill varying  
284 between 0.8 m and 1.8 m in depressions. Clay illuviation was more pronounced in the upper

285 part of the hillslope (higher gradient in clay content) indicating lower conductivities in deeper  
286 soil layers.

## 287 **2.5 Modeling**

### 288 **2.5.1 The Catchment Modeling Framework (CMF)**

289 The Catchment Modeling Framework (CMF) developed by Kraft et al. (2011) is a modular  
290 hydrological model based on the concept of finite volume method introduced by Qu and  
291 Duffy (2007). Within CMF those finite volumes (e.g. soil water storages, streams) are linked  
292 by a series of flow accounting equations (e.g. Richards or Darcy equation) to a one to three  
293 dimensional representation of the real world hydrological system. The flexible set up of CMF  
294 and the variety of available flow accounting equations allows customizing the setup as  
295 required in the presented study. In addition to the water fluxes, the advective movement of  
296 tracers within a given system can be accounted for by CMF, making this modeling framework  
297 especially suitable to be used in our tracer study (Kraft et al., 2010). Starting with Beven and  
298 Germann (1982) scientist over the last decades frequently argued that Richards equation like  
299 flow accounting equation assuming a time invariant and well mixed homogenous flow of  
300 water through the soil pore space, similar to those currently implemented in CMF, are not  
301 suitable to account for preferential flow relevant for modeling tracer transport (Brooks et al.,  
302 2010; Germann et al., 2007; Hrachowitz et al., 2013; Stumpp and Maloszewski, 2010). Being  
303 developed for the quantitative representation of soil water flow this equations cannot  
304 distinguish between water stored in different soil compartments (namely the soil matrix and  
305 macro pores) and only artificially try to represent macropore flow e.g. by favoring high  
306 saturated conductivity values or misshaped conductivity curves controlling the flow of water  
307 between soil compartments. Even though the capabilities of CMF to account for preferential  
308 flow are still in the development phase (e.g. by following the dual permeability approach in  
309 the future) and are not accounted for in the presented setup, our setup will once more

310 highlight potential draw backs of the modeling approaches relying on Richards equation while  
311 modeling tracer transport at the hillslope scale.

### 312 2.5.2 Setup of CMF

313 To govern the water fluxes within our system we used the following flow accounting  
314 equations: Manning equation for surface water flow; Richards equation for a full 2-D  
315 representation of the subsurface flow; Shuttleworth-Wallace modification (Shuttleworth and  
316 Wallace, 1985) of the Penman-Monteith method to control evaporation and transpiration;  
317 constant Dirichlet boundary conditions representing the groundwater table and the outlet of  
318 the system as a rectangular ditch with a depth of 1.5 m. The lower boundary condition is only  
319 applicable if groundwater table is >2 m below ground. Preliminary testing revealed that a  
320 discretization based on a constant vertical shift (5m) and alternating cell width increasing  
321 width depth (ranging from 1.25 cm to 83.75 cm) yielded the optimum model performance  
322 with regard to computing time and model quality. Based on 5 m contour lines (derived by  
323 local LIDAR measurements with a raster resolution of 1 m; using the Spatial Analyst package  
324 of ArcGis 10.1 from ESRI) this hillslope was further separated into 32 cells ranging in size  
325 from 16.6 m<sup>2</sup> to 2,921.6 m<sup>2</sup> (Figure 1a). To account for small scale dynamics in the mixing  
326 process of stable water isotopes and to be able to run the model with a satisfactory speed, two  
327 different horizontal resolutions were used to discretize the each layer with depth. Layers  
328 encompassing wick samplers and their upslope neighbor were run with a finer resolution of at  
329 least 26 virtual soil layers increasing in thickness width depth (1x1.25 cm, 13 x 2.5 cm,  
330 7 x 5 cm and 5 x 10-50 cm). All other cells were calculated with coarser resolution of at least  
331 14 virtual soil layers (1 x 1.25 cm, 1 x 2.5 cm, 6 x 5 cm, 3 x 10 cm and 3 x 15-83.75 cm). In  
332 case the delineated soil type changed within a soil layer it was further subdivided according to  
333 Figure 2.

### 334 | **2.5.3 Evapotranspiration**

335 Soil evaporation, evaporation of intercepted water and plant transpiration are calculated  
336 separately using the sparse canopy evapotranspiration method by Shuttleworth and Wallace  
337 (1985), in its modification by Federer et al. (2003) and Kraft et al. (2011). This approach  
338 requires the following parameterizations: soil surface wetness dependent resistance to extract  
339 water from the soil ( $r_{ss}$ ), the plant type dependent bulk stomatal resistance to extract water  
340 from the leaves ( $r_{sc}$ ), the aerodynamic resistances parameters ( $r_{aa}$ ,  $r_{as}$ , and  $r_{ac}$ ) for sparse crops  
341 as described by Shuttleworth and Gurney (1990) and Federer et al. (2003). Whereby  $r_{ac}$   
342 (Resistance Canopy Atmosphere) restricts the vapor movement between the leaves and the  
343 zero plane displacement height and  $r_{as}$  (Resistance Soil Atmosphere) restricts the vapor  
344 movement between the soil surface and the zero plane displacement height, which is the  
345 height of the mean canopy flow (Shuttleworth and Wallace, 1985; Thom, 1972). The  
346 aerodynamic resistances parameter  $r_{aa}$  refers to the resistance to move vapor between the zero  
347 plane displacement height and the reference height at which the available measurements were  
348 made. The necessary assumptions to parameterize the plant (*Setaria sphacelata*) and soil  
349 dependent parameters of the Shuttleworth-Wallace equation using the assumptions made by  
350 Federer et al. (2003) and Kraft et al. (2011) are listed in Tab. 2.

351 Furthermore, soil water extraction by evaporation is only affecting the top soil layer and soil  
352 water extraction by transpiration is directly controlled by root distribution at a certain soil  
353 depth. In accordance with field observations, we assumed an exponential decay of root mass  
354 with depth, whereby 90 % of the total root mass is concentrated in the top 0.20 m.

355

### 356 | **2.5.4 Calibration & Validation**

357 For calibration and validation purposes, we compared measured and modeled stable water  
358 isotope signatures of  $^2\text{H}$  and  $^{18}\text{O}$  of the soil water at each depths of the each wick sampler

359 along the modeled hillslope. Hourly values of the modeled isotopic soil water signature were  
360 aggregated to represent the mean isotopic composition in between measurements ( $\approx 7$  days)  
361 and are reported in per mil relative to the Vienna Standard Mean Ocean Water (VSMOW)  
362 (Craig, 1961).

363 Literature and measured values for soil and plant parameters (Tab. 1 and Tab. 2) were used to  
364 derive the initial values for the calibration process. The initial states for calibration were  
365 retrieved by artificially running the model with those initial values for the first 2 years of the  
366 available dataset (Tab. 3). The results of this pre-calibration run were used as a starting point  
367 for all following calibration runs. A warm up period of 4 month (1.7.2010-31.10.10) preceded  
368 the calibration period (1.11.2010-31.10.2011) to adjust the model to the new parameter set.  
369 To simulate a wide range of possible flow conditions and limit the degrees of freedom for the  
370 possible model realizations we selected  $K_{\text{sat}}$  and porosity for calibration, while the *Van*  
371 *Genuchten-Mualem* parameters remained constant since measured pF curves where available.  
372 Even though not all sensitive parameters of the Richards equation controlling the flow regime  
373 where accounted for during the calibration process, we assume that the measured *Van*  
374 *Genuchten-Mualem* parameters alpha and n are in the good agreement with the actual flow  
375 characteristics of the soils. As typical for the application of the VanGenuchten - Mualem  
376 approach the tortuosity/connectivity coefficient remained constant throughout all model runs  
377 with a value of 0.5. Beside the 4 soil parameters shown in Tab. 1 and the upper and lower the  
378 boundary conditions, only the 9 parameters of the Shuttleworth-Wallace equation Tab. 2 had  
379 to be set prior to each model run. To further control the unknown lower boundary condition  
380 and complement the calibration process, the suction induced by groundwater depth was  
381 changed for each calibration run.

382 To increase the efficiency of the calibration runs and evenly explore the given parameter  
383 space we used the Latin-Hyper cube method presented by McKay et al. (1979). The parameter

384 range of each variable was therefore subdivided into 10 strata and sampled once using  
385 uniform distribution. All strata are then randomly matched to get the final parameter sets. A  
386 total of  $10^5$  parameter sets were generated for calibration with varying values for  $K_{sat}$  and  
387 porosity for all 8 soil types as well as different groundwater depths. An initial trial using  $10^4$   
388 parameter sets was used to narrow down the parameter range as specified in Tab. 4 for  $K_{sat}$   
389 and porosity for all 8 soil types and to 0 m to 100 m for the applicable groundwater depths.  
390 The performance of each parameter set was evaluated based on the goodness-of-fit criteria  
391 Nash-Sutcliffe efficiency (NSE) and the coefficient of determination ( $R^2$ ). In addition, the  
392 bias was calculated as an indicator for any systematic or structural deviation of the model.  
393 After the calibration the best performing (“behavioral”) models according to a  $NSE > 0.15$ , an  
394 overall bias  $< \pm 20.0 \%$   $\delta^2H$  and a coefficient of determination  $R^2 > 0.65$ , were used for the  
395 validation period (Tab. 3) using the final states of the calibration period as initial values.

### 396 **3 Results and discussion**

#### 397 **3.1 Model performance**

398 In order to quantify the flow processes we first validated the overall suitability of the chosen  
399 model approach and the performance of the parameter sets. The parameter sets best  
400 representing the isotope dynamics of  $\delta^2H$  (as previously defined as best performing  
401 (“behavioral”) parameter sets; same accounts for  $\delta^{18}O$ ; results are not shown) during the  
402 calibration period, explained the observed variation to even a higher degree during the  
403 validation period (average NSE 0.19 for calibration versus 0.35 for validation).

404 The linear correlation between modeled and observed isotope dynamics of  $\delta^2H$ , for the best  
405 performing parameter sets, were equally good during the calibration and validation period  
406 ( $R^2 \approx 0.66$ ) (Tab. 5). The goodness-of-fit criteria for the single best performing parameter set  
407 (“best model fit”) shows an  $R^2$  of 0.84 and a NSE of 0.42.

408 Figure 3 depicts the measured and modeled temporal development of the soil water isotope  
409 profile along the studied hillslope as well as the  $\delta^2\text{H}$  signature and amount of the incoming  
410 rainfall used to drive the model. The measured temporal delay of the incoming signal with  
411 depth and the general seasonal pattern of the  $\delta^2\text{H}$  signal are captured by the model (Figure 3).

412 The bias was negative throughout all model realizations during calibration and validation (-  
413 15.90 ( $\pm 0.11$  SD) ‰  $\delta^2\text{H}$  and -16.93 ( $\pm 0.34$  SD) ‰  $\delta^2\text{H}$  respectively see Tab. 5). Even though  
414 the high bias indicates a structural insufficiency of the model, we are confident that this can  
415 be mostly attributed by the discrimination of evaporation processes at the soil-atmosphere  
416 interface and on the canopy.

417 | Our first hypothesis-I, that evaporation in general plays only a minor role for the soil water  
418 | isotope cycle under full vegetation, therefore needs to be reconsidered. Even though  
419 | hypothesis I has previously been frequently used as an untested assumption for various  
420 | models (e.g. Vogel et al., 2010; Dohnal et al., 2012) it is rarely scrutinized under natural  
421 | conditions. A complete rejection of Completely rejecting this hypothesis could therefore  
422 | affect the interpretations in those studies and limit their applicability fundamentally. However,  
423 | further studies are needed to support these findings and before finally rejecting this  
424 | hypothesis. The lateral mixing processes maybe obscuring the observed near surface  
425 | enrichment and the effect of preferential flow currently not fully accounted for could further  
426 | hinder the full interpretation of these findings. It still holds true, that:

- 427 - the quantitative loss due to surface evaporation on areas with a high leaf area index is  
428 more or less insignificant (accounting for 38 mm a<sup>-1</sup> out of 1,896 mm a<sup>-1</sup>;  $\approx 2\%$ ; Figure 5),
- 429 - the isotopic enrichment due to evaporation for vegetated areas is considerably lower than  
430 for non-vegetated areas, as previously shown by Dubbert et al. (2013), and
- 431 - high rainfall intensity constrains any near surface isotopic enrichment related to  
432 evaporation (Hsieh et al., 1998).

433 However, our results indicate that the contribution of potential canopy evaporation  
434 (accounting for 344 mm a<sup>-1</sup> out of 1,896 mm a<sup>-1</sup>; ≈18%; Figure 5) to enrich the canopy storage  
435 and thereby potential throughfall (discriminating <sup>18</sup>O and <sup>2</sup>H resulting in more positive isotope  
436 signatures) still could partially explain the observed bias.

437 Nevertheless we presume that fog drip, created by sieving bypassing clouds or radiation fog  
438 frequently occurring in the study area Bendix et al. (2008), explains the majority of the  
439 observed bias. Depending on the climatic processes generating the fog drip is typically  
440 isotopically enriched compared to rainfall, due to different condensation temperatures (Scholl  
441 et al., 2009). To get an impression for the magnitude of the possible bias due to throughfall  
442 and fog drip compared to direct rainfall, we compare the observed bias with a study presented  
443 by Liu et al. (2007) conducted in a tropical seasonal rain forest in China. They observed an  
444 average enrichment of +5.5 ‰ δ<sup>2</sup>H for throughfall and +45.3 ‰ δ<sup>2</sup>H for fog drip compared  
445 to rainfall. Even though the observed enrichment of fog drip and throughfall by Liu et al.  
446 (2007) may not be as pronounced within our study area (Goller et al., 2005), the general  
447 tendency could explain the modeled bias. According to Bendix et al. (2008) fog and cloud  
448 water deposition within our study area contributes 121 mm a<sup>-1</sup> to 210 mm a<sup>-1</sup> at the respective  
449 elevation. Assessing the actual amount fog drip for grass species like *Setaria sphacelata*  
450 under natural conditions is challenging and has so far not been accounted for.

451 In case that further discrimination below the surface would substantially alter the isotope  
452 signature, the bias would change continuously with depth. Any subsurface flow reaching wick  
453 samplers at lower elevations would then further increase the bias. However, the negative bias  
454 of -16.19 (±2.80 SD) ‰ δ<sup>2</sup>H in all monitored top wick samplers during validation accounts  
455 for most of the observed bias in the two deeper wick samplers amounting to  
456 -17.32 (±2.47 SD) ‰ δ<sup>2</sup>H. Thus we conclude that the bias is mainly a result of constraints  
457 related to modeling surface processes, rather than subsurface ones.

458 Figure 4 shows the behavior of the chosen parameter sets for saturated hydraulic conductivity  
459 and groundwater depth during calibration and validation. The parameter space allows us to  
460 assess the range of suitable parameters and their sensitivity over a given parameter range.  
461 During calibration the given parameter space could not be constrained to more precise values  
462 for all parameters, which in this case should show a lower SD (Tab. 6) and narrower box plots  
463 (Figure 4). Especially the  $K_{\text{sat}}$  values of the soil layers A1, A3 and B1-B3, the porosity for all  
464 soil layers (not included in Figure 4) and the groundwater depth depict a low sensitive over  
465 the entire calibration range (indicated by a high SD, wide box plot, and evenly scattered  
466 points; Tab. 6 and Figure 4). In particular the low sensitivity of the model towards  
467 groundwater depth seems surprising, but can be explained by the potentially low saturated  
468 hydraulic conductivities of the lower soil layers C1 and C2 limiting the percolation into the  
469 lower soil layers outside of the modeling domain. Even an extreme hydraulic potential,  
470 induced by a deep groundwater body, can be limited by a low hydraulic conductivity. None  
471 the less it noteworthy, that no model run without an active groundwater body as a lower  
472 boundary condition (groundwater depth < 2 m) results in a model performance with  $\text{NSE} > 0$   
473 (Figure 4). With a groundwater depth above 2 m the boundary condition would serve as a  
474 source of water with an undefined isotopic signal and prevent any percolation of water into  
475 deeper soil layers outside of the modeling domain. The results are therefore in alignment with  
476 the topography of the system indicating an active groundwater body deeper than 2 m and  
477 support our second hypothesis which we will further discuss in section 3.2. We identified  
478 several parameter combinations showing the same model performance, known as equifinality  
479 according to Beven and Freer (2001). The observed equifinality can partially be explained by  
480 counteracting effects of a decreasing  $K_{\text{sat}}$  and an increasing pore space, or that the water flow  
481 is restrained due to lower hydraulic conductivities at adjoining soil layers. Especially for  
482 deeper soil layers the interaction between surrounding layers makes it especially difficult to  
483 further constrain the given parameter range. Even though the parameter ranges for all

484 behavioral model realizations are not so well confined, the small confidence intervals indicate  
485 a certain degree of robustness towards the predicted flows (Figure 3). Additional soil moisture  
486 measurements complementing the current setup in the future will allow us to put further  
487 confidence in this new approach and the drawn conclusions and allow us to directly compare  
488 different calibration targets (i.e. soil moisture vs. soil water isotopic signature).

489 Initial  $K_{\text{sat}}$  values based on literature values (see Tab. 1) deviate to a large extent from those  
490 derived through the calibration process. This is attributable to the occurrence of preferential  
491 flow within the macro pores (Bronstert and Plate, 1997) and the sampling method (PCaps)  
492 used to extract the soil water ~~mostly~~ stored in the soil with a matrix potential up to 30 hPa in  
493 the macropores (Landon et al., 1999). It becomes apparent that the mixing processes (based  
494 on dispersion and molecular diffusion) are not sufficient to equilibrate the isotope signature  
495 over the entire pore space (Landon et al., 1999; Šimůnek et al., 2003) and that the flow  
496 through the pore space is not homogenous. Thus the isotopic signature between the sampled  
497 pore media and the total modeled pore space differs (Brooks et al., 2010; Hrachowitz et al.,  
498 2013; McDonnell and Beven, 2014; McGlynn et al., 2002). The model tries to account for  
499 these effects by favoring high  $K_{\text{sat}}$  values during calibration (McDonnell and Beven, 2014;  
500 McGlynn et al., 2002).

501 Modeling soil water movement under such conditions should therefore be used with caution  
502 for models based on Darcy-Richards equation which assume instantaneously homogeneous  
503 mixed solutions and uniform flow. In line with the argumentation started by Beven and  
504 Germann (1982) and refreshed in their recent paper Beven and Germann (2013) we therefore  
505 stress the importance to account for preferential flow processes and overcome the limitation  
506 of Darcy-Richards equation limiting the explanatory power of hydrological models predicting  
507 water flow and solute/isotope transport in particular. Like Gerke (2006) and Šimůnek and van  
508 Genuchten (2008) among others we therefore seek to implement a dual permeability approach

509 accounting for different flow patterns within the soil pore space ([Gerke, 2006](#); [Jarvis, 2007](#);  
510 [Šimůnek and van Genuchten, 2008](#); [Vogel et al., 2000, 2006, 2010](#)). In the style of existing 1-  
511 Dmodels for soil water isotope transport presented by Braud et al. (2005) and Haverd and  
512 Cuntz (2010) the inter-soil mixing processes by dispersion and molecular diffusion between  
513 different soil pore space compartments shall be accounted for in the future. Based on the  
514 presented findings this can now be extended towards the development and application of soil  
515 water isotope models under natural conditions. To conclude, the results highlight the general  
516 suitability of high resolution soil water isotope profiles to improve our understanding of  
517 subsurface water flux separation implemented in current hillslope model applications and to  
518 predict subsurface soil water movement.

### 519 **3.2 Modeled water fluxes**

520 Acknowledging the general suitability of the model to delineate the prevailing flow patterns,  
521 we will now compare those to the current hydrological process understanding presented in the  
522 introduction. Figure 5 depicts the water balance of the modeled hillslope based on all  
523 behavioral model realizations, separating the amount of incoming precipitation into the main  
524 flow components: surface runoff and subsurface flow directly entering the stream, percolation  
525 to groundwater and evapotranspiration.

526 Evapotranspiration is further subdivided into transpiration and evaporation from the soil  
527 surface and the canopy, whereby evaporation from the canopy is designated as interception  
528 losses. Due to the small confidence intervals of the behavioral model runs (see Figure 3) the  
529 standard deviations of the model's flow components are relatively small (see Figure 5;  
530 [standard deviation and mean value was computed without weighting the likelihood value](#)).

531 The observed order of magnitude for evapotranspiration is in good agreement with previous  
532 values of 945 and 876 mm a<sup>-1</sup> reported for tropical grasslands by Windhorst et al. (2013a) and  
533 Oke (1987), respectively. As previously mentioned the evaporation of 382 mm a<sup>-1</sup> is

534 dominated by interception losses accounting for  $344 \text{ mm a}^{-1}$ . Overall, these results support  
535 hypothesis II, which stated that a large share of the incoming precipitation is routed through  
536 the deeper soil layer and/or the groundwater body (here 49.7% or  $942 \text{ mm a}^{-1}$ ) before it enters  
537 the stream. This also explains the long mean transit time of water of around 1.0 to 3.9 years  
538 (Crespo et al., 2012; Timbe et al., 2014) in comparison to the fast runoff reaction time. Well  
539 in agreement with our current process understanding and hypothesis III, we can further show  
540 that the occurrence of surface runoff ( $33 \text{ mm a}^{-1}$ ) due to Hortonian overland flow is less  
541 important. For the graphical representation the surface runoff has therefore been combined  
542 with subsurface flow ( $2 \text{ mm a}^{-1}$ ) to “surface runoff & subsurface flow”, accounting in total for  
543  $35 \text{ mm a}^{-1}$  (see Figure 5). A more heterogeneous picture can be depicted if we take a closer  
544 look at the flow processes along the studied hillslope and its soil profiles (Figure 6).

545 Vertical fluxes still dominate the flow of water (Figure 6b), but the near surface lateral flow  
546 components predicted by Bückner et al. (2010) become more evident (Figure 6a). Explained by  
547 the high saturated hydraulic conductivities in the top soil layers (Tab. 6 and Figure 4) up to  
548  $7.3 \cdot 10^3 \text{ m}^3 \text{ a}^{-1}$  are transported lateral between cells in the top soil layer, referring to 15.6% of  
549 the total flow leaving the system per year. According to the model results deep lateral flow is  
550 minimal accounting only for <0.1% of the total flow. It only occurs on top of the deeper soil  
551 horizons with low  $K_{\text{sat}}$  values. For all behavioral model realizations the groundwater level was  
552 >2 m thereby limiting the direct contribution of subsurface flow ( $2 \text{ mm a}^{-1}$ ) to the tributary,  
553 which had a hydraulic potential of only 1.5 m. Over the entire hillslope the importance of  
554 overland flow remains below 3% ( $\approx 50 \text{ mm a}^{-1}$ ), of which a part is re-infiltrating, summing up  
555 to total overland flow losses of around 2% at the hillslope scale ( $35 \text{ mm a}^{-1}$ , Figure 5). These  
556 results demonstrate the importance of near surface lateral flow and hence support hypothesis  
557 IV.

#### 558 **4 Conclusion**

559 These data and findings support and complement the existing process understanding mainly  
560 gained by Goller et al. (2005), Fleischbein et al. (2006) Boy et al. (2008), Bücken et al.  
561 (2010), Crespo et al. (2012) and Timbe et al. (2014) to a large extent. Moreover, it was  
562 possible to quantify for the first time the relevance of near surface lateral flow generation. The  
563 observed dominance of vertical percolation into the groundwater body and thereby the  
564 importance of preferential flow seems to be quite common for humid tropical montane  
565 regions and has recently been reported by Muñoz-Villers & McDonnell (2012) in a similar  
566 environment.

567 Being aware of the rapid rainfall-runoff response of streams within the catchment of the Rio  
568 San Francisco it has been questioned whether and how the system can store water for several  
569 years and still release it within minutes. Throughout the last decades several studies have  
570 observed similar hydrological behavior especially for steep humid montane regions (e.g.  
571 McDonnell (1990) and Muñoz-Villers & McDonnell (2012)) and concepts have been  
572 developed to explain this behavior: e.g. piston flow (McDonnell, 1990), kinematic waves  
573 (Lighthill and Whitham, 1955), transmissivity feedback (Kendall et al., 1999). Due to the  
574 limited depth of observations (max. depth 0.4 m) and the low overall influence of the lateral  
575 flows a more exact evaluation of the fate of the percolated water is still not possible.  
576 However, we are confident, that in combination with a suitable concept to account for the  
577 rapid mobilization of the percolated water into a tributary and experimental findings, further  
578 refining possible model realizations an improved version of the current approach, could  
579 further close the gap in our current process understanding.

580 Over decades hydrological models which are based on the Richards or Darcy equation (like  
581 the one we used), have been tuned to predict quantitative flow processes and mostly been  
582 validated using soil moisture data suitable to account for overall storage changes. Our results  
583 imply that doing this considerably well does not necessarily mean that the models actually

584 transport the *right* water at the *right* time. Using tracer data to validate models as we did  
585 entails that those models now not only have to transport the correct amount but additionally  
586 the *right* water. Consequently, the relevance of the correct representation of uneven  
587 preferential flow through pipes or macropores, which is misleadingly compensated by high  
588 conductivities over the entire pore space within models based on the Richards or Darcy  
589 equation, becomes immense. Distinguishing between water flowing in different compartments  
590 (e.g. pipes, cracks and macro pores) of the soil is a key task to get a closer and more precise  
591 representation of the natural flow processes. Even though the chosen modeling structure  
592 currently lacks a sufficient robustness to be widely applicable it highlights the potential and  
593 future research directions for soil water isotope modeling.

594 **Acknowledgments**

595  
596 The current study was conducted within the DFG Research Group FOR 816 “Biodiversity and  
597 sustainable management of a megadiverse mountain rain forest in south Ecuador” and the  
598 follow-up project PAK 825/3. The authors are very grateful for the funding supplied by the  
599 German Research Foundation DFG (BR2238/4-2 and BR 2238/14-1) and thank Thorsten  
600 Peters of the University of Erlangen for providing meteorological data.

601

602 **References**

- 603 Barthold, F.K., Tyralla, C., Schneider, K., Vaché, K.B., Frede, H.-G., Breuer, L., 2011. How  
604 many tracers do we need for end member mixing analysis (EMMA)? A sensitivity  
605 analysis. *Water Resour. Res.* 47, W08519. doi:10.1029/2011WR010604
- 606 Beck, E., Makeschin, F., Haubrich, F., Richter, M., Bendix, J., Valerezo, C., 2008. The  
607 Ecosystem (Reserva Biológica San Francisco), in: Beck, E., Bendix, J., Kottke, I.,  
608 Makeschin, F., Mosandl, R. (Eds.), *Gradients in a Tropical Mountain Ecosystem of*  
609 *Ecuador, Ecological Studies.* Springer Berlin Heidelberg, pp. 1–13.
- 610 Bendix, J., Rollenbeck, R., Richter, M., Fabian, P., Emck, P., 2008. Climate, in: Beck, E.,  
611 Bendix, J., Kottke, I., Makeschin, F., Mosandl, R. (Eds.), *Gradients in a Tropical*  
612 *Mountain Ecosystem of Ecuador, Ecological Studies.* Springer Berlin Heidelberg, pp.  
613 63–73.
- 614 Bendix, J., Silva, B., Roos, K., Göttlicher, D.O., Rollenbeck, R., Nauß, T., Beck, E., 2010.  
615 Model parameterization to simulate and compare the PAR absorption potential of two  
616 competing plant species. *Int. J. Biometeorol.* 54, 283–295. doi:10.1007/s00484-009-  
617 0279-3
- 618 Beven, K., Germann, P., 1982. Macropores and water flow in soils. *Water Resour. Res.* 18,  
619 1311–1325. doi:10.1029/WR018i005p01311
- 620 Beven, K., Germann, P., 2013. Macropores and water flow in soils revisited. *Water Resour.*  
621 *Res.* 49, 3071–3092. doi:10.1002/wrcr.20156
- 622 Bogner, C., Bauer, F., Trancón y Widemann, B., Viñan, P., Balcazar, L., Huwe, B., 2014.  
623 Quantifying the morphology of flow patterns in landslide-affected and unaffected  
624 soils. *J. Hydrol.* 511, 460–473. doi:10.1016/j.jhydrol.2014.01.063
- 625 Boy, J., Valarezo, C., Wilcke, W., 2008. Water flow paths in soil control element exports in  
626 an Andean tropical montane forest. *Eur. J. Soil Sci.* 59, 1209–1227.  
627 doi:10.1111/j.1365-2389.2008.01063.x
- 628 Braud, I., Bariac, T., Gaudet, J.P., Vauclin, M., 2005. SiSPAT-Isotope, a coupled heat, water  
629 and stable isotope (HDO and H218O) transport model for bare soil. Part I. Model  
630 description and first verifications. *J. Hydrol.* 309, 277–300.  
631 doi:10.1016/j.jhydrol.2004.12.013
- 632 Bronstert, A., 1999. Capabilities and limitations of detailed hillslope hydrological modelling.  
633 *Hydrol. Process.* 13, 21–48. doi:10.1002/(SICI)1099-1085(199901)13:1<21::AID-  
634 HYP702>3.0.CO;2-4

635 Bronstert, A., Plate, E.J., 1997. Modelling of runoff generation and soil moisture dynamics for  
636 hillslopes and micro-catchments. *J. Hydrol.* 198, 177–195. doi:10.1016/S0022-  
637 1694(96)03306-9

638 Brooks, J.R., Barnard, H.R., Coulombe, R., McDonnell, J.J., 2010. Ecohydrologic separation  
639 of water between trees and streams in a Mediterranean climate. *Nat. Geosci.* 3, 100–  
640 104. doi:10.1038/ngeo722

641 Bücken, A., Crespo, P., Frede, H.-G., Breuer, L., 2011. Solute behaviour and export rates in  
642 neotropical montane catchments under different land-uses. *J. Trop. Ecol.* 27, 305–317.  
643 doi:10.1017/S0266467410000787

644 Bücken, A., Crespo, P., Frede, H.-G., Vaché, K., Cisneros, F., Breuer, L., 2010. Identifying  
645 Controls on Water Chemistry of Tropical Cloud Forest Catchments: Combining  
646 Descriptive Approaches and Multivariate Analysis. *Aquat. Geochem.* 16, 127–149.  
647 doi:10.1007/s10498-009-9073-4

648 Colman, R.L., Wilson, G.P.M., 1960. The Effect of Floods on Pasture Plants. *Agric. Gaz.*  
649 NSW 71, 337–347.

650 Craig, H., 1961. Standard for Reporting Concentrations of Deuterium and Oxygen-18 in  
651 Natural Waters. *Science* 133, 1833–1834. doi:10.1126/science.133.3467.1833

652 Craig, H., Gordon, L.I., 1965. Deuterium and oxygen 18 variations in the ocean and the  
653 marine atmosphere, in: Tongiogi, E. (Ed.), *Proceedings of the Conference on the*  
654 *Stable Isotopes in Oceanographic Studies and Paleotemperatures.* Lishi e F., Pisa,  
655 Spoleto, Italy, pp. 9–130.

656 Crespo, P., Bücken, A., Feyen, J., Vaché, K.B., Frede, H.-G., Breuer, L., 2012. Preliminary  
657 evaluation of the runoff processes in a remote montane cloud forest basin using  
658 Mixing Model Analysis and Mean Transit Time. *Hydrol. Process.* 26, 3896–3910.  
659 doi:10.1002/hyp.8382

660 Davies, J., Beven, K., Rodhe, A., Nyberg, L., Bishop, K., 2013. Integrated modeling of flow  
661 and residence times at the catchment scale with multiple interacting pathways. *Water*  
662 *Resour. Res.* 49, 4738–4750. doi:10.1002/wrcr.20377

663 Dohnal, M., Vogel, T., Šanda, M., Jelínková, V., 2012. Uncertainty Analysis of a Dual-  
664 Continuum Model Used to Simulate Subsurface Hillslope Runoff Involving Oxygen-  
665 18 as Natural Tracer. *J. Hydrol. Hydromech.* 60, 194–205. doi:10.2478/v10098-012-  
666 0017-0

667 Dubbert, M., Cuntz, M., Piayda, A., Maguás, C., Werner, C., 2013. Partitioning  
668 evapotranspiration – Testing the Craig and Gordon model with field measurements of  
669 oxygen isotope ratios of evaporative fluxes. *J. Hydrol.* 496, 142–153.  
670 doi:10.1016/j.jhydrol.2013.05.033

671 Federer, C.A., Vörösmarty, C., Fekete, B., 2003. Sensitivity of Annual Evaporation to Soil  
672 and Root Properties in Two Models of Contrasting Complexity. *J. Hydrometeorol.* 4,  
673 1276–1290. doi:10.1175/1525-7541(2003)004<1276:SOAETS>2.0.CO;2

674 Fleischbein, K., Wilcke, W., Valarezo, C., Zech, W., Knoblich, K., 2006. Water budgets of  
675 three small catchments under montane forest in Ecuador: experimental and modelling  
676 approach. *Hydrol. Process.* 20, 2491–2507. doi:10.1002/hyp.6212

677 Frisbee, M.D., Phillips, F.M., Campbell, A.R., Hendrickx, J.M.H., 2010. Modified passive  
678 capillary samplers for collecting samples of snowmelt infiltration for stable isotope  
679 analysis in remote, seasonally inaccessible watersheds 1: laboratory evaluation.  
680 *Hydrol. Process.* 24, 825–833. doi:10.1002/hyp.7523

681 Garvelmann, J., Külls, C., Weiler, M., 2012. A porewater-based stable isotope approach for  
682 the investigation of subsurface hydrological processes. *Hydrol Earth Syst Sci* 16, 631–  
683 640. doi:10.5194/hess-16-631-2012

684 Genereux, D.P., Hooper, R.P., 1999. Oxygen and hydrogen isotopes in rainfall-runoff studies,  
685 in: Kendall, C., McDonnell, J.J. (Eds.), *Isotope Tracers in Catchment Hydrology*.  
686 Elsevier, pp. 319–346.

687 Gerke, H.H., 2006. Preferential flow descriptions for structured soils. *J. Plant Nutr. Soil Sci.*  
688 169, 382–400. doi:10.1002/jpln.200521955

689 Germann, P., Helbling, A., Vadilonga, T., 2007. Rivulet Approach to Rates of Preferential  
690 Infiltration. *Vadose Zone J.* 6, 207. doi:10.2136/vzj2006.0115

691 Goller, R., Wilcke, W., Leng, M.J., Tobschall, H.J., Wagner, K., Valarezo, C., Zech, W.,  
692 2005. Tracing water paths through small catchments under a tropical montane rain  
693 forest in south Ecuador by an oxygen isotope approach. *J. Hydrol.* 308, 67–80.  
694 doi:10.1016/j.jhydrol.2004.10.022

695 Hacker, J.B., Jones, R.J., 1969. The *Setaria sphacelata* complex - a review. *Trop. Grassl.* 3,  
696 13–34.

697 Haverd, V., Cuntz, M., 2010. Soil–Litter–Iso: A one-dimensional model for coupled transport  
698 of heat, water and stable isotopes in soil with a litter layer and root extraction. *J.*  
699 *Hydrol.* 388, 438–455. doi:10.1016/j.jhydrol.2010.05.029

700 Hrachowitz, M., Savenije, H., Bogaard, T.A., Tetzlaff, D., Soulsby, C., 2013. What can flux  
701 tracking teach us about water age distribution patterns and their temporal dynamics?  
702 *Hydrol Earth Syst Sci* 17, 533–564. doi:10.5194/hess-17-533-2013

703 Hsieh, J.C., Chadwick, O.A., Kelly, E.F., Savin, S.M., 1998. Oxygen isotopic composition of  
704 soil water: Quantifying evaporation and transpiration. *Geoderma* 82, 269–293.  
705 doi:10.1016/S0016-7061(97)00105-5

706 Hunter, J.D., 2007. Matplotlib: A 2D Graphics Environment. *Comput. Sci. Eng.* 9, 90–95.  
707 doi:10.1109/MCSE.2007.55

708 Huwe, B., Zimmermann, B., Zeilinger, J., Quizhpe, M., Elsenbeer, H., 2008. Gradients and  
709 Patterns of Soil Physical Parameters at Local, Field and Catchment Scales, in: Beck,  
710 E., Bendix, J., Kottke, I., Makeschin, F., Mosandl, R. (Eds.), *Gradients in a Tropical*  
711 *Mountain Ecosystem of Ecuador, Ecological Studies*. Springer Berlin Heidelberg, pp.  
712 375–386.

713 Jarvis, N.J., 2007. A review of non-equilibrium water flow and solute transport in soil  
714 macropores: principles, controlling factors and consequences for water quality. *Eur. J.*  
715 *Soil Sci.* 58, 523–546. doi:10.1111/j.1365-2389.2007.00915.x

716 Kendall, K.A., Shanley, J.B., McDonnell, J.J., 1999. A hydrometric and geochemical  
717 approach to test the transmissivity feedback hypothesis during snowmelt. *J. Hydrol.*  
718 219, 188–205. doi:10.1016/S0022-1694(99)00059-1

719 Kirkby, M., 1988. Hillslope runoff processes and models. *J. Hydrol.* 100, 315–339.  
720 doi:10.1016/0022-1694(88)90190-4

721 Körner, C., Scheel, J., Bauer, H., 1979. Maximum leaf diffusive conductance in vascular  
722 plants. *Photosynthetica* 13, 45–82.

723 Kraft, P., Multsch, S., Vaché, K.B., Frede, H.-G., Breuer, L., 2010. Using Python as a  
724 coupling platform for integrated catchment models. *Adv. Geosci.* 27, 51–56.  
725 doi:10.5194/adgeo-27-51-2010

726 Kraft, P., Vaché, K.B., Frede, H.-G., Breuer, L., 2011. CMF: A Hydrological Programming  
727 Language Extension For Integrated Catchment Models. *Environ. Model. Softw.* 26,  
728 828–830. doi:10.1016/j.envsoft.2010.12.009

729 Landon, M.K., Delin, G.N., Komor, S.C., Regan, C.P., 1999. Comparison of the stable-  
730 isotopic composition of soil water collected from suction lysimeters, wick samplers,  
731 and cores in a sandy unsaturated zone. *J. Hydrol.* 224, 45–54. doi:10.1016/S0022-  
732 1694(99)00120-1

733 Leibundgut, C., Maloszewski, P., Külls, C., 2011. *Tracers in Hydrology*. John Wiley & Sons,  
734 Chichester, UK.

- 735 Lighthill, M.J., Whitham, G.B., 1955. On Kinematic Waves. II. A Theory of Traffic Flow on  
736 Long Crowded Roads. *Proc. R. Soc. Lond. Ser. Math. Phys. Sci.* 229, 317–345.  
737 doi:10.1098/rspa.1955.0089
- 738 Liu, W.J., Liu, W.Y., Li, P.J., Gao, L., Shen, Y.X., Wang, P.Y., Zhang, Y.P., Li, H.M., 2007.  
739 Using stable isotopes to determine sources of fog drip in a tropical seasonal rain forest  
740 of Xishuangbanna, SW China. *Agric. For. Meteorol.* 143, 80–91.  
741 doi:10.1016/j.agrformet.2006.11.009
- 742 McDonnell, J.J., 1990. A Rationale for Old Water Discharge Through Macropores in a Steep,  
743 Humid Catchment. *Water Resour. Res.* 26, 2821–2832.  
744 doi:10.1029/WR026i011p02821
- 745 McDonnell, J.J., Beven, K., 2014. Debates—The future of hydrological sciences: A  
746 (common) path forward? A call to action aimed at understanding velocities, celerities  
747 and residence time distributions of the headwater hydrograph. *Water Resour. Res.* 50,  
748 5342–5350. doi:10.1002/2013WR015141
- 749 McDonnell, J.J., Sivapalan, M., Vaché, K., Dunn, S., Grant, G., Haggerty, R., Hinz, C.,  
750 Hooper, R., Kirchner, J., Roderick, M.L., Selker, J., Weiler, M., 2007. Moving beyond  
751 heterogeneity and process complexity: A new vision for watershed hydrology. *Water*  
752 *Resour. Res.* 43, W07301. doi:10.1029/2006WR005467
- 753 McGlynn, B.L., McDonnell, J.J., Brammer, D.D., 2002. A review of the evolving perceptual  
754 model of hillslope flowpaths at the Maimai catchments, New Zealand. *J. Hydrol.* 257,  
755 1–26. doi:10.1016/S0022-1694(01)00559-5
- 756 McKay, M.D., Beckman, R.J., Conover, W.J., 1979. A Comparison of Three Methods for  
757 Selecting Values of Input Variables in the Analysis of Output from a Computer Code.  
758 *Technometrics* 21, 239–245. doi:10.2307/1268522
- 759 McMillan, H., Tetzlaff, D., Clark, M., Soulsby, C., 2012. Do time-variable tracers aid the  
760 evaluation of hydrological model structure? A multimodel approach. *Water Resour.*  
761 *Res.* 48, W05501. doi:10.1029/2011WR011688
- 762 Mertens, J., Diels, J., Feyen, J., Vanderborght, J., 2007. Numerical analysis of Passive  
763 Capillary Wick Samplers prior to field installation. *Soil Sci. Soc. Am. J.* 71, 35–42.  
764 doi:10.2136/sssaj2006.0106
- 765 Muñoz-Villers, L.E., McDonnell, J.J., 2012. Runoff generation in a steep, tropical montane  
766 cloud forest catchment on permeable volcanic substrate. *Water Resour. Res.* 48,  
767 W09528. doi:10.1029/2011WR011316
- 768 Oke, T.R., 1987. *Boundary Layer Climates*, 2nd ed. Methuen, London, UK.
- 769 Qu, Y., Duffy, C.J., 2007. A semidiscrete finite volume formulation for multiprocess  
770 watershed simulation. *Water Resour. Res.* 43, W08419. doi:10.1029/2006WR005752
- 771 Rhoades, C.C., Eckert, G.E., Coleman, D.C., 2000. Soil carbon differences among forest,  
772 agriculture, and secondary vegetation in lower montane Ecuador. *Ecol. Appl.* 10, 497–  
773 505. doi:10.1890/1051-0761(2000)010[0497:SCDAFA]2.0.CO;2
- 774 Scholl, M.A., Shanley, J.B., Zegarra, J.P., Coplen, T.B., 2009. The stable isotope amount  
775 effect: New insights from NEXRAD echo tops, Luquillo Mountains, Puerto Rico.  
776 *Water Resour. Res.* 45, W12407. doi:10.1029/2008WR007515
- 777 Shuttleworth, W.J., Gurney, R.J., 1990. The theoretical relationship between foliage  
778 temperature and canopy resistance in sparse crops. *Q. J. R. Meteorol. Soc.* 116, 497–  
779 519. doi:10.1002/qj.49711649213
- 780 Shuttleworth, W.J., Wallace, J.S., 1985. Evaporation from sparse crops—an energy  
781 combination theory. *Q. J. R. Meteorol. Soc.* 111, 839–855.  
782 doi:10.1002/qj.49711146910
- 783 Šimůnek, J., Jarvis, N.J., van Genuchten, M.T., Gärdenäs, A., 2003. Review and comparison  
784 of models for describing non-equilibrium and preferential flow and transport in the  
785 vadose zone. *J. Hydrol.* 272, 14–35. doi:10.1016/S0022-1694(02)00252-4

786 Šimůnek, J., van Genuchten, M.T., 2008. Modeling Nonequilibrium Flow and Transport  
787 Processes Using HYDRUS. *Vadose Zone J.* 7, 782–797. doi:10.2136/vzj2007.0074  
788 Sklash, M.G., Farvolden, R.N., Fritz, P., 1976. A conceptual model of watershed response to  
789 rainfall, developed through the use of oxygen-18 as a natural tracer. *Can. J. Earth Sci.*  
790 13, 271–283. doi:10.1139/e76-029  
791 Soulsby, C., Rodgers, P., Smart, R., Dawson, J., Dunn, S., 2003. A tracer-based assessment of  
792 hydrological pathways at different spatial scales in a mesoscale Scottish catchment.  
793 *Hydrol. Process.* 17, 759–777. doi:10.1002/hyp.1163  
794 Stumpff, C., Maloszewski, P., 2010. Quantification of preferential flow and flow  
795 heterogeneities in an unsaturated soil planted with different crops using the  
796 environmental isotope  $\delta^{18}\text{O}$ . *J. Hydrol.* 394, 407–415.  
797 doi:10.1016/j.jhydrol.2010.09.014  
798 Tetzlaff, D., McDonnell, J.J., Uhlenbrook, S., McGuire, K.J., Bogaart, P.W., Naef, F., Baird,  
799 A.J., Dunn, S.M., Soulsby, C., 2008. Conceptualizing catchment processes: simply too  
800 complex? *Hydrol. Process.* 22, 1727–1730. doi:10.1002/hyp.7069  
801 Thom, A.S., 1972. Momentum, mass and heat exchange of vegetation. *Q. J. R. Meteorol. Soc.*  
802 98, 124–134. doi:10.1002/qj.49709841510  
803 Timbe, E., Windhorst, D., Crespo, P., Frede, H.-G., Feyen, J., Breuer, L., 2014.  
804 Understanding uncertainties when inferring mean transit times of water trough tracer-  
805 based lumped-parameter models in Andean tropical montane cloud forest catchments.  
806 *Hydrol. Earth Syst. Sci.* 18, 1503–1523. doi:10.5194/hess-18-1503-2014  
807 Uhlenbrook, S., Roser, S., Tilch, N., 2004. Hydrological process representation at the meso-  
808 scale: the potential of a distributed, conceptual catchment model. *J. Hydrol.* 291, 278–  
809 296. doi:10.1016/j.jhydrol.2003.12.038  
810 Vogel, H.-J., Cousin, I., Ippisch, O., Bastian, P., 2006. The dominant role of structure for  
811 solute transport in soil: experimental evidence and modelling of structure and transport  
812 in a field experiment. *Hydrol Earth Syst Sci* 10, 495–506. doi:10.5194/hess-10-495-  
813 2006  
814 Vogel, T., Gerke, H.H., Zhang, R., Van Genuchten, M.T., 2000. Modeling flow and transport  
815 in a two-dimensional dual-permeability system with spatially variable hydraulic  
816 properties. *J. Hydrol.* 238, 78–89. doi:10.1016/S0022-1694(00)00327-9  
817 Vogel, T., Sanda, M., Dusek, J., Dohnal, M., Votrubova, J., 2010. Using Oxygen-18 to Study  
818 the Role of Preferential Flow in the Formation of Hillslope Runoff. *Vadose Zone J.* 9,  
819 252–259. doi:10.2136/vzj2009.0066  
820 Weiler, M., McDonnell, J., 2004. Virtual experiments: a new approach for improving process  
821 conceptualization in hillslope hydrology. *J. Hydrol.* 285, 3–18. doi:10.1016/S0022-  
822 1694(03)00271-3  
823 Wheeler, M.D., Newman, S.M., Orr-Ewing, A.J., Ashfold, M.N.R., 1998. Cavity ring-down  
824 spectroscopy. *J. Chem. Soc. Faraday Trans.* 94, 337–351. doi:10.1039/A707686J  
825 Windhorst, D., Brenner, S., Peters, T., Meyer, H., Thies, B., Bendix, J., Frede, H.-G., Breuer,  
826 L., 2013a. Impacts of Local Land-Use Change on Climate and Hydrology, in: Bendix,  
827 J., Beck, E., Bräuning, A., Makeschin, F., Mosandl, R., Scheu, S., Wilcke, W. (Eds.),  
828 *Ecosystem Services, Biodiversity and Environmental Change in a Tropical Mountain*  
829 *Ecosystem of South Ecuador, Ecological Studies Vol. 221.* Springer, Berlin,  
830 Heidelberg, New York, pp. 275–286.  
831 Windhorst, D., Waltz, T., Timbe, E., Frede, H.-G., Breuer, L., 2013b. Impact of elevation and  
832 weather patterns on the isotopic composition of precipitation in a tropical montane  
833 rainforest. *Hydrol. Earth Syst. Sci.* 17, 409–419. doi:10.5194/hess-17-409-2013  
834 Zimmermann, B., Elsenbeer, H., 2008. Spatial and temporal variability of soil saturated  
835 hydraulic conductivity in gradients of disturbance. *J. Hydrol.* 361, 78–95.  
836 doi:10.1016/j.jhydrol.2008.07.027

837 Zimmermann, U., Ehhalt, D., Muennich, K.O., 1968. Soil-Water Movement and  
838 Evapotranspiration: Changes in the Isotopic Composition of the Water., in: Isotopes in  
839 Hydrology. International Atomic Energy Agency, Vienna, pp. 567–585.  
840  
841

842 **Tables**843 **Tab. 1 Soil physical parameters**

Soil code	Clay [%]	Texture			Porosity [%]	$K_{sat}^*$ [m/d]	Van Genuchten- Mualem Parameters	
		Sand [%]	Silt [%]	$\alpha$			$n$	
A1 & A1 top	34	17	49	81	0.324	0.641	1.16	
A2 & A2 top	19	33	49	63	0.324	0.352	1.13	
A3 & A3 top	15	34	51	74	0.324	0.221	1.24	
B1	8	16	76	66	0.228	1.046	1.19	
B2	15	34	51	59	0.228	0.145	1.13	
B3	11	18	70	58	0.228	0.152	1.16	
C1	15	45	40	55	0.026	0.023	1.12	
C2	45	20	35	47	0.026	0.004	1.17	

\* $K_{sat}$  values are based on values taken within the proximity of the hillslope under similar land use by Crespo et al. (2012) and Zimmermann and Elsenbeer (2008).

844

845 **Tab. 2 Plant (*Setaria sphacelata*) and soil dependent parameters used for the Shuttleworth-Wallace equation**

Parameter	Symbol	Value	Unit	Used to calculate	Source
<b>Potential soil surface resistance</b>	$r_{ss\ pot}$	500	$s\ m^{-1}$	$r_{ss}$	Federer et al.(2003)
<b>Max. stomatal conductivity or max. leaf conductance</b>	$g_{max}$	270	$s\ m^{-1}$	$r_{sc}$	Körner et al. (1979)
<b>Leaf area index</b>	LAI	3.7	$m^2\ m^{-2}$	$r_{sc}$	Bendix et al. (2010)
<b>Canopy height</b>	h	0.2	m	$r_{aa}, r_{ac}$ & $r_{as}$	Estimate based on hand measurements
<b>Representative leaf width</b>	w	0.015	m	$r_{ac}$	
<b>Extinction coefficient for photosynthetically active radiation in the canopy</b>	CR	70	%	$r_{sc}$	Federer et al.(2003)
<b>Canopy storage capacity</b>	-	0.15	$mm\ LAI^{-1}$	Interception	Federer et al.(2003)
<b>Canopy closure</b>	-	90	%	Throughfall	Estimate based on image evaluation
<b>Albedo</b>	alb	11,7	%	Net radiation	Bendix et al. (2010)

846

847

848 Tab. 3 Modeling periods

Description	Period		Duration [days]
	Start	End	
<b>Initial states</b>	1 July 2010	30 June 2012	730
<b>Warm up period</b>	1 July 2010	31 October 2010	122
<b>Calibration period</b>	1 November 2010	31 October 2011	364
<b>Validation period</b>	1 November 2011	31 October 2012	365

849

850 Tab. 4 Soil parameter ranges for the Monte Carlo simulations ([assuming uniform distribution for each parameter](#)).

Soil code	$K_{sat}$ [ $m\ d^{-1}$ ]		Porosity [ $m^3\ m^{-3}$ ]	
	Min.	Max.	Min.	Max.
A1-3 top	0.001	35	0.3	0.9
A1-3	0.001	30	0.3	0.9
B1-3	0.001	12	0.1	0.8
C1-2	0.001	8	0.1	0.8

851

852 Tab. 5 Model performance during calibration and validation for all behavioral model runs (based on all calibration  
853 runs with  $NSE > 0.15$ ,  $bias < \pm 20.0\%$   $\delta^2H$  and  $R^2 > 0.65$ ). Best modeled fit based on NSE.

	Calibration 2010-2011		Validation 2011-2012		Best modeled fit
	Mean	SD	Mean	SD	
<b>NSE</b>	0.19	0.008	0.35	0.029	0.42
<b>R<sup>2</sup></b>	0.67	0.008	0.66	0.020	0.84
<b>Bias</b>	-15.90	0.113	-16.93	0.344	-16.16

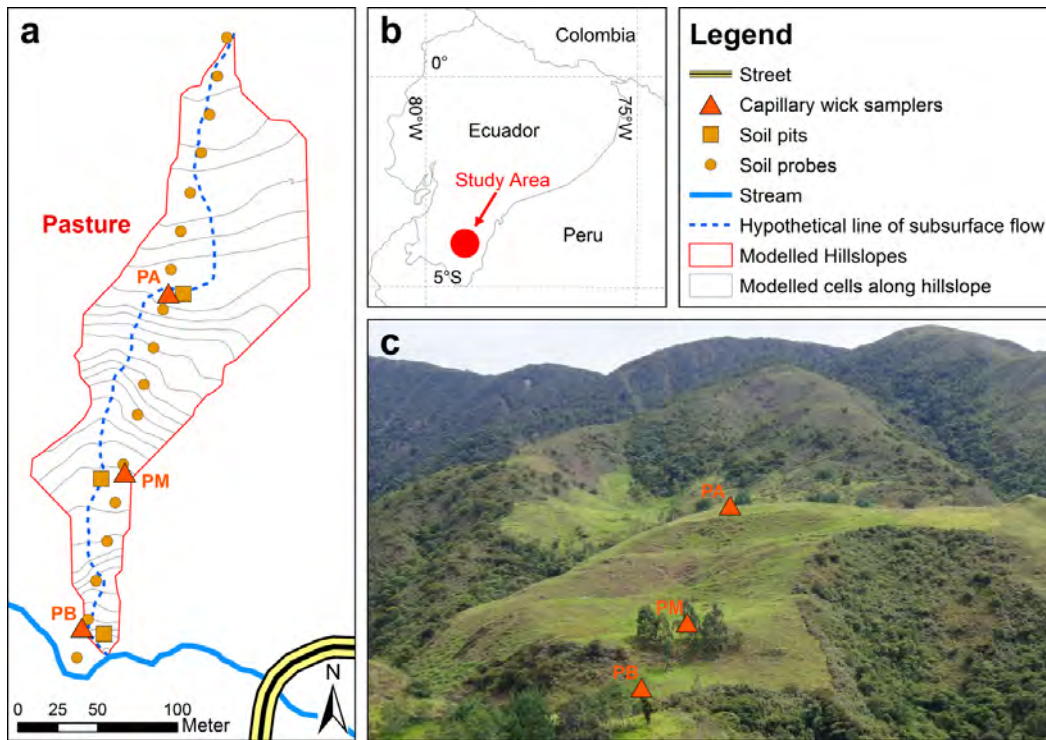
854

855  
856

**Tab. 6** Parameter ranges used for validation (all calibration runs with NSE>0.15, bias< $\pm$ 20.0 ‰  $\delta^2\text{H}$  and  $R^2 > 0.65$ ) and parameter set for the best modeled fit based on NSE.

	Mean	SD	Best modeled fit
<b><math>K_{\text{sat}}</math> [<math>\text{m d}^{-1}</math>]</b>			
A1 top	21.8	5.8	20.4
A2 top	11.0	2.3	12.6
A3 top	25.6	6.3	29.6
A1	11.7	6.6	13.5
A2	7.4	2.8	8.9
A3	15.7	6.4	15.3
B1	4.0	2.4	4.0
B2	5.2	3.2	10.5
B3	4.6	2.2	2.5
C1	1.3	1.2	0.6
C2	1.7	1.4	0.1
<b>Porosity [<math>\text{m}^3 \text{m}^{-3}</math>]</b>			
A1 top	0.54	0.08	0.44
A2 top	0.56	0.09	0.44
A3 top	0.66	0.09	0.53
A1	0.55	0.08	0.42
A2	0.55	0.09	0.46
A3	0.65	0.09	0.74
B1	0.34	0.09	0.31
B2	0.64	0.09	0.54
B3	0.75	0.09	0.70
C1	0.54	0.09	0.41
C2	0.55	0.09	0.67
<b>Groundwater depth [m]</b>			
	50.5	28.6	76.5

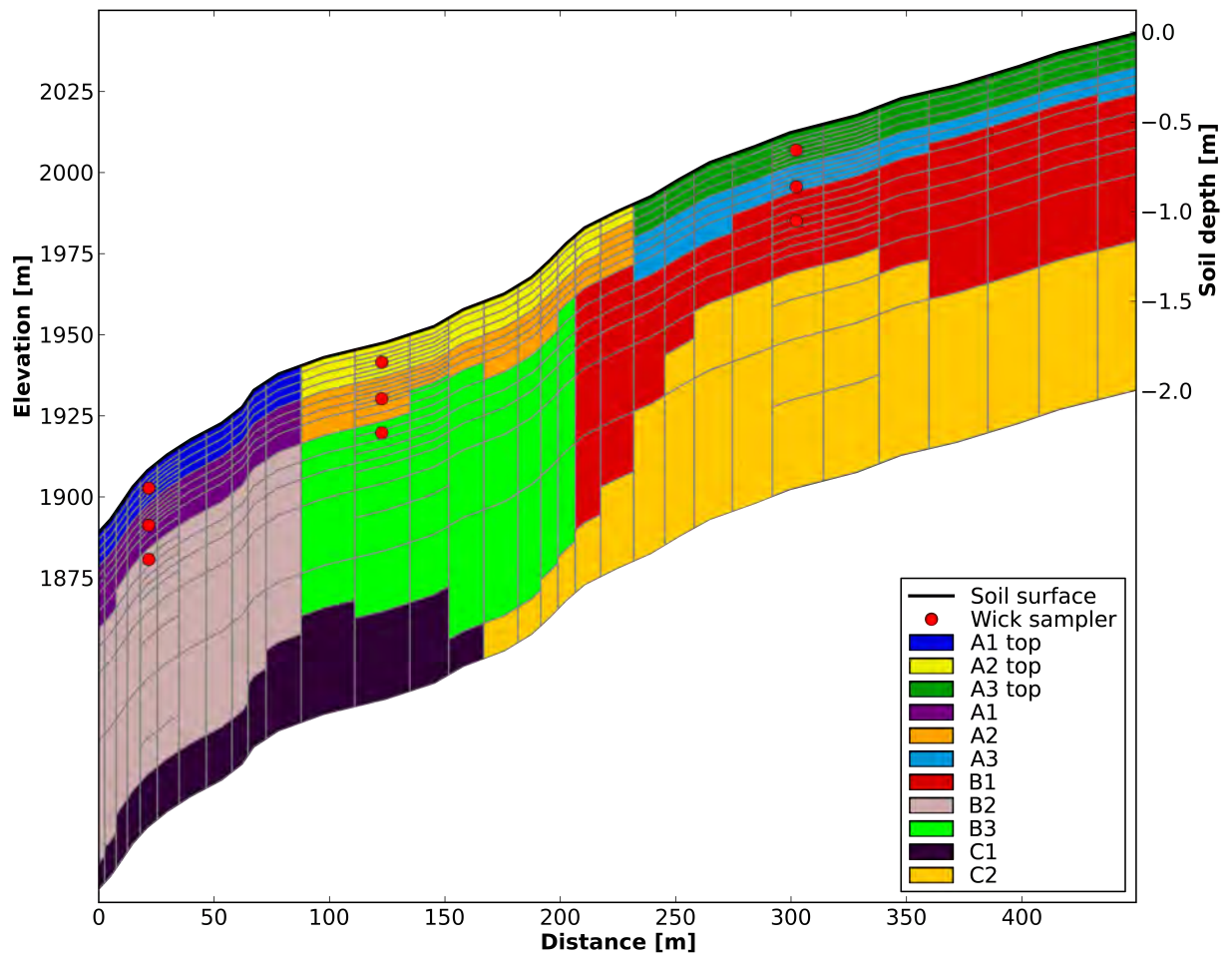
857



859

860 **Figure 1** a) Outline of the modeled hillslope and its virtual discretization into cells. b) Location of the study area  
 861 within Ecuador c) Photograph showing the Location of the wick samplers (P = Pasture and B = bajo/lower  
 862 level, M = medio/middle level, A = alto/top level sampler).

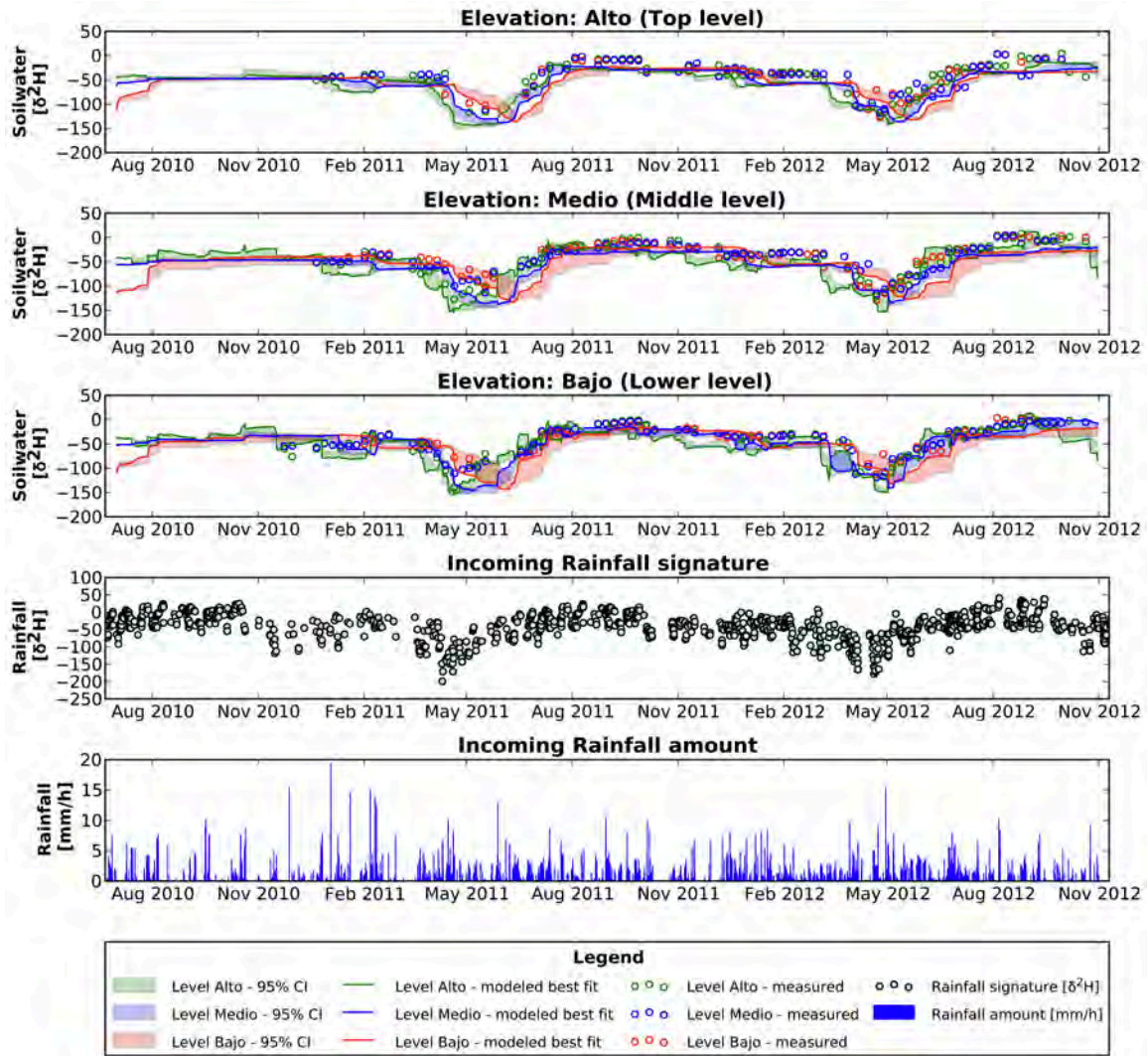
863



864

865 **Figure 2** Elevation profile (top black line, left ordinate), succession of soil layer types (color plate) and soil depths  
 866 assigned to the modeling grid (right ordinate).

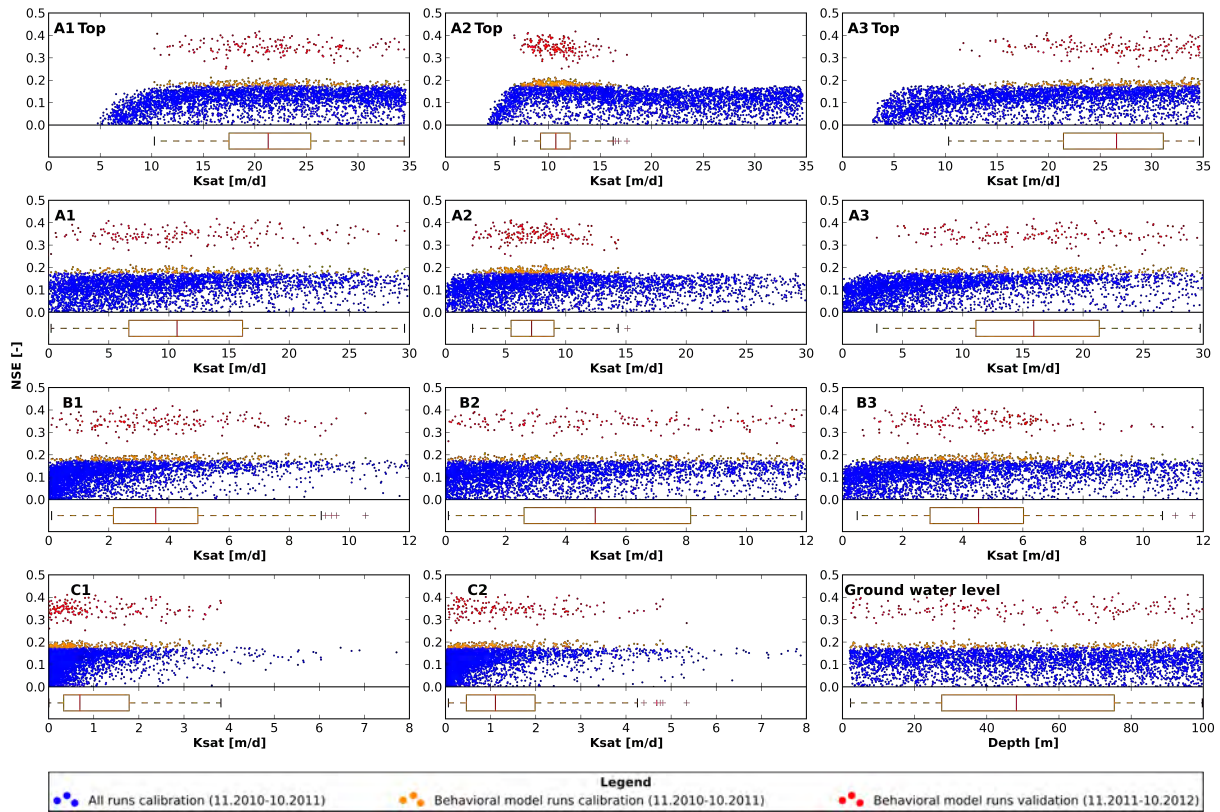
867



868

869 Figure 3 Time series of soil water isotope signatures (Top panels 1-3 for each elevation) for all behavioral model runs  
 870 with:  $NSE > 0.15$ ,  $bias < \pm 20.0 \text{ ‰ } \delta^2H$  and  $R^2 > 0.65$  showing the 95% confidence interval (CI; transparent  
 871 areas) and best modeled fit (solid line) vs. measured values (circles) at all 3 elevations (2,010, 1,949 and  
 872 1,904 m a.s.l.) and soil depths below ground (0.10, 0.25 and 0.40 m). Bottom panels 4 and 5, isotopic  
 873 signature and rainfall amount, respectively.

874

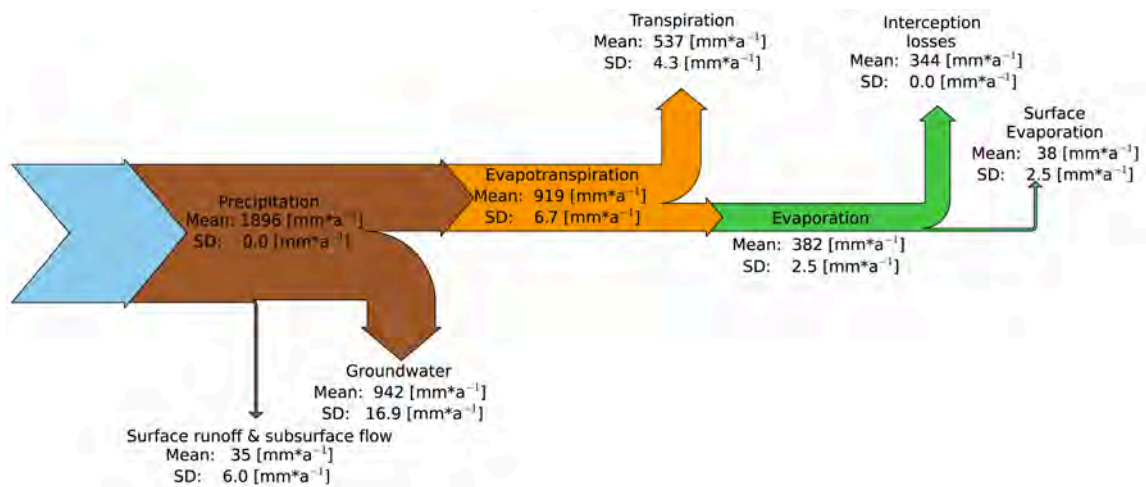


875

876 Figure 4 Dotty plots of NSE values ( $>0.0$ ) during calibration (blue) and for behavioral model runs ( $NSE > 0.15$ , bias  
 877  $< \pm 20.0\%$   $\delta^2H$  and  $R^2 > 0.65$ ) during calibration (orange) and validation (red) for saturated hydraulic  
 878 conductivity ( $K_{sat}$ ) for all soil types and groundwater depth. Box plots show the unweighted parameter  
 879 distribution of all behavioral model runs ( $NSE > 0.15$ , bias  $< \pm 20.0\%$   $\delta^2H$  and  $R^2 > 0.65$ ) ~~used for validation~~.  
 880 Results for soil porosity look similar to those of the groundwater and are therefore not shown.

881

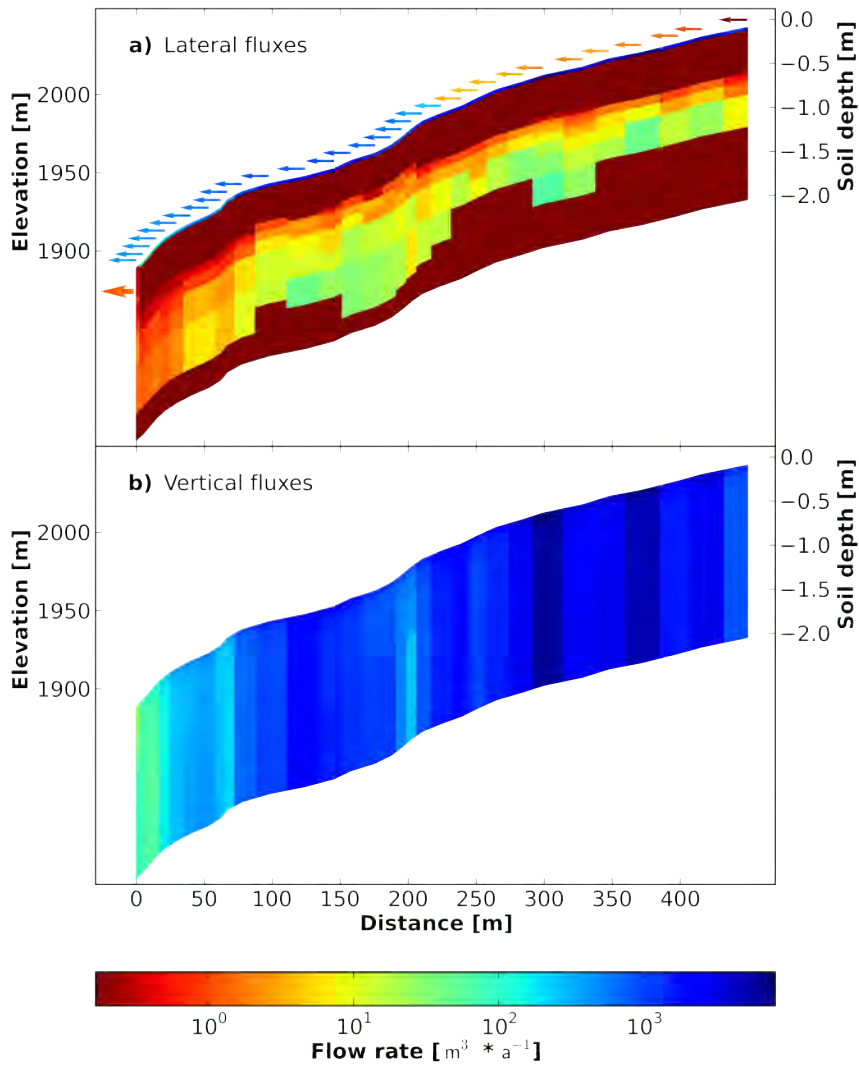
882



883

884 Figure 5 Mean annual flows and standard deviation (SD) of the main flow components at a hillslope scale of all  
 885 behavioral model runs from 2010-2012.

886



887

888 **Figure 6 a) Lateral and b) vertical fluxes for the best modeled fit. Arrows indicate the amount of surface runoff and**  
 889 **direct contribution to the outlet through subsurface flow. The maximum flow between storage compartments**  
 890 **is  $7.3 \cdot 10^3 \text{ m}^3 \text{ a}^{-1}$  and the total observed flow leaving as well as entering the system accumulates to  $37 \cdot 10^3 \text{ m}^3 \text{ a}^{-1}$ .**  
 891

892